ONLINE ESTIMATION OF THE ROAD GRADE AND THE GROSS WEIGHT OF AN ELECTRIC DRIVE SHUTTLE BASED ON LONGITUDINAL VEHICLE DYNAMICS

by

Hasan Atacan Tosun

Submitted to the Graduate School of Engineering and Natural Sciences
in partial fulfillment of
the requirements for the degree of Master of Science

SABANCI UNIVERSITY

December, 2024

Online Estimation of The Road Grade and The Gross Weight of
an Electric Drive Shuttle Based on Longitudinal Vehicle Dynamics

Hasan Atacan Tosun

Mechatronics Engineering, M.Sc. Thesis, 2024

Thesis Supervisor: Asst. Prof. Dr. Melih Türkseven

Keywords: Vehicle mass estimation, road grade estimation, online estimation, gradient descent, RLS (Recursive Least Square), real-time estimation, vehicle longitudinal dynamics, commercial electric vehicle

Abstract

The vehicle mass and road grade have significant influences on the longitudinal dynamics of commercial vehicles for passenger transportation, such as buses and shuttles. Therefore, estimating these factors plays an important role in both controlling the vehicle's motion and estimating its total energy consumption. The road grade varies as the vehicle moves, and the gross weight of a shuttle changes during a trip due to the number of passengers on board, which requires an online estimation that can track these changes during the operation. The challenge of making accurate online estimations has usually been overcome by placing additional sensors on the vehicle and incorporating sensor fusion techniques.

This study investigates the efficacy of conventional online parameter estimation approaches, specifically Gradient Descent and Recursive Least Squares in estimating the road grade and vehicle mass without utilizing any sensors except the ones typically included in standard commercial vehicles. A commercially available electric drive shuttle was converted into a test bed, and the performance of the proposed methods was evaluated under actual road conditions with varying gross weights. The results indicated that the estimation performance is highly sensitive to model accuracy, warranting further study on identifying prominent factors that affect the longitudinal dynamics of the vehicle.

Elektrikli Bir Servis Aracının Yokuş Eğimi ve Brüt Ağırlığının Boylamasına Araç Dinamiklerine Dayalı Çevrimiçi Tahmini

Hasan Atacan Tosun

Mekatronik Mühendisliği, Yüksek Lisans Tezi, 2024

Tez Danışmanı: Asst. Prof. Dr. Melih Türkseven

Anahtar kelimeler: Araç ağırlık tahmini, yol eğimi tahmini, çevrimiçi tahmini, gradyan azalma, özyinelemeli/indirgemeli/ardışık en küçük kareler, gerçek zamanlı tahmin, boylamasına araç dinamiği, ticari elektrikli araç

Özet

Araç kütlesi ve yol eğimi, yolcu taşımacılığı için kullanılan otobüsler ve servis araçları gibi ticari araçların boyuna dinamikleri üzerinde önemli bir etkiye sahiptir. Bu nedenle, bu faktörlerin tahmin edilmesi, hem aracın hareketinin kontrol edilmesinde hem de toplam enerji tüketiminin tahmin edilmesinde önemli bir rol oynamaktadır. Yol eğimi, araç hareket ettikçe değişmekte, servisin brüt ağırlığı ise yolculuk sırasında taşıdığı yolcu sayısına bağlı olarak farklılık göstermektedir. Bu durum, operasyon sırasında bu değişiklikleri takip edebilecek çevrimiçi bir tahmin sistemi gerektirmektedir. Doğru çevrimiçi tahminler yapmak genellikle araca ek sensörler yerleştirilmesi ve sensör füzyon tekniklerinin kullanılmasıyla sağlanmıştır.

Bu çalışma, yol eğimi ve araç kütlesini tahmin etmek için, standart ticari araçlarda genellikle bulunan sensörler dışında başka sensörler kullanmaksızın, geleneksel çevrimiçi parametre tahmin yaklaşımlarının, özellikle gradyan azalma ve özyinelemeli / indirgemeli / ardışık en küçük kareler yöntemlerinin etkinliğini araştırmaktadır. Temin edilen ticari elektrikli bir servis aracı, test aracına dönüştürülmüş ve incelenen yöntemlerin performansı, değişen brüt ağırlıklarla gerçek yol koşullarında test edilmiştir. Sonuçlar, tahmin performansının model doğruluğuna oldukça duyarlı olduğunu göstermiş ve aracın boyuna dinamiklerini etkileyen önemli faktörlerin belirlenmesi üzerine daha fazla çalışmanın gerekliliğini ortaya koymuştur.

Acknowledgements

First and foremost, I would like to express my gratitude to my thesis advisor, Dr. Melih Türkseven for his unwavering guidance and support during graduate studies at Sabancı University.

His expertise has not only enriched my academic career, but also his support and endless motivation significantly contributed to the completion of this thesis.

Furthermore, I am deeply grateful to the members of my thesis jury, Prof. Mustafa Ünel and Dr. Masoud Latifinavid, for generously dedicating their time to serve on my thesis committee and for their invaluable advice and feedback. Also, I would like to thank Dr. Hamit Tekin and Dr. Matin Ghaziani for guidance and contributions to academic journey.

I extend my heartfelt appreciation to my beloved parents Zuhal Tosun and Sinan Tosun for their endless support throughout my studies, without which I could not have become the person, engineer, and researcher I am today.

I am grateful to my colleagues from the Mechatronics Laboratory, namely Burak Aladağ, Bilal Çatkın, Ilhami Osman Karakurt, Umut Barut, Emre Yavaş, Harun Tolasa, Özgür Taylan Kenanoğlu, Görkem Gemalmaz, Ahmet Faruk Günalp, Alperen Kenan and Mehmet Emin Mumcuoğlu for the enjoyable moments shared and the countless coffees together.

I wish to express my gratitude to my bachelor's friends, Mehmet Özkan Demir, Ömer Selek, Melih Güden, Utku Bıçakcı, Serkan Yapar, Anıl Karatopak, Can Akyol, Ufuk Liman, Nihat Uzgan, Cihangir Aladoğan and Kubilay Baş who have been by my side for over a decade.

Special thanks go to my friends Mert Yaşar and Ömer Faruk Yeter for their friendship, unwavering support and guidance whenever needed.

I would like to thank my grandmother Safiye Tosun, who was with me for much of my childhood and youth, and for her patience with me. I fondly remember the unforgettable breakfasts, the playful chases, the stories, and all the enjoyable times we shared.

Finally, I would like to express my gratitude to KARSAN Automotive for supporting me throughout my studies, to my esteemed manager Nurettin Özekmekci

for providing me with these opportunities, and to Mustafa Alper Balım for his unwavering support and encouragement.

to my beloved mom...

Contents

List of Figures

List of Tables

Chapter 1

Introduction

1.1 Context and Motivation

In 2022, transportation activities accounted for 31% of the EU total energy consumption [6] and, 74% of all energy consumption is associated with road transport. In addition to that, over 25% of greenhouse gas emissions from road transport in the EU are attributed to the heavy-duty vehicle (HDV) sector. Based on the regulation 2024/1610 of the European Parliament and council, from 2025 all HDV manufacturers must comply with fleet-wide CO2 emissions standards for approval of new HDVs. The purpose of this regulation is to reduce emissions in order to meet the 2030 objectives and achieve climate neutrality for Europe by 2050.

Battery electric (BEV) and hybrid electric vehicles (HEV) with enhanced energy storage system (ESS) and propulsion system efficiency, these domains on which we can concentrate and observe enhancement especially, consumption and range estimation, during the period of transition time.

The inertia of the vehicle including vehicle mass is affecting both the prediction of energy consumption and the model of the vehicle dynamics. So, getting it right would improve both planning the energy-saving motion and control of the vehicle. In [7], the research examines energy requirements for various vehicle categories, including the Nissan Micra (Category B), Audi A2 and Peugeot 106, along commuter

routes between Bristol and Bath, utilizing both empirical data and simulations. Substantial assumptions were established for comparisons, including route characteristics, traffic circumstances, and vehicle tonnage. The energy demands of rolling resistance, aerodynamic drag, inertial acceleration, gravitational losses, and cornering forces were determined by a parametric model. The results indicated that the energy demand of the B class vehicle decreases by 6–8% when the mass of the vehicle is reduced by 10%. Road gradient also significantly affected efficiency, with hilly routes such as the Upper Bristol Road causing higher gravity and cornering losses, while flatter routes provided the advantage of lower aerodynamic losses at higher speeds.

Road grades are even more influential (compared to mass) on energy cost. A 1% change in the road grade results in a 15% increase in the energy required for maintaining the speed of the vehicle. A 6% road grade doubles the consumption [7]. Therefore, a motion planner that can take road grade into account could reduce the energy consumption by modulating the target speed of the vehicle online. For example, in [8], cruise controlling with and without taking road grade into account resulted in a 5% saving in energy and 42% reduction in gear shift. In order to optimize fuel efficiency, the investigation concentrates on a Scania heavy-duty diesel vehicle that has been assessed through simulations and real-world highway tests. It utilizes a dynamic programming (DP) technique within a look-ahead control (LC) framework, including GPS and on-board road slope data to optimize the truck's velocity trajectory. This predictive controller dynamically modifies speed according to road conditions, resulting in considerable fuel savings. The traditional cruise control (CC), which sustains a steady pace without adjusting for road inclines, acts as a standard for comparison. In contrast to CC, LC incorporates the DP technique to predict and change speed, surpassing CC in fuel efficiency and trip optimization by utilizing road geometry data in both simulated and actual environments.

1.2 An Overview of Estimation Techniques

1.2.1 Recursive Least Squares (RLS)

The Recursive Least Squares algorithm is a well-established method in vehicle dynamics that allows for the real-time estimation of critical parameters, including vehicle mass and road grade. The studies that were reviewed demonstrate the application and advancements of RLS, with a particular emphasis on its integration with longitudinal and lateral vehicle dynamics to improve the accuracy of estimation. Longitudinal dynamics encompass aspects like aerodynamic drag, rolling resistance, and road gradient effects, whereas involve tire forces, slip angles, and steering behavior examples of lateral dynamics. This comprehensive approach ensures robust parameter estimation across diverse operational conditions. Kim et al. [9] employed Recursive Least Squares to estimate vehicle mass during both straight-line and lateral maneuvers with single forgetting factor, applied for both gradient and mass analyses. Their research utilized simulations to develop and evaluate estimation algorithms, achieving error margins of less than 5% in dynamic conditions. Additionally, the study verified torque-based and sensor-based approaches for estimating road grade on a Hyundai-Kia YF Sonata Hybrid. Performance was precise across grades of up to 20%, as indicated by the results.

McIntyre et al. [10] present a significant two-stage estimation algorithm for determining vehicle mass and road grade, specifically targeting heavy-duty vehicles (2009). Initially, an adaptive least-squares algorithm devoid of a forgetting factor determines the vehicle's weight. Assuming the mass estimate is precise, a nonlinear estimator accounts for the time-varying road gradient in the subsequent step. The method attained an error of under 5% in mass estimation within 20 seconds and accurately monitored road grade fluctuations with a root-mean square error of about 0.55.

The research confirmed the method via simulations and empirical testing on heavy-duty trucks. Vehicles with varied payloads and specified mass configurations were

employed in scientific experiments along multiple routes, while simulations incorporated sinusoidal and step fluctuations in road grade. This dual-phase system showed significant efficiency in use scenarios, tackling issues such as inconsistent acceleration data and fluctuating vehicle conditions. Vahidi et al. [11] proposed a Recursive Least Squares approach using several forgetting factors for the real-time estimation of vehicle mass and road gradient. By devoting distinct forgetting factors to mass (fixed) and grade (time-varying), the algorithm overcame the difficulty of estimating parameters with inconsistent rates of variation. The test was performed on a Freightliner heavy-duty truck with a mass of roughly 20 tons (21,250 kg) and the methodology was corroborated using simulations and real-world test environment. Simulations featured step and sinusoidal fluctuations in road grade, while empirical tests were performed on a 12 km segment of Interstate 15 in San Diego, characterized by varied road gradients and payload conditions.

The test conditions included driving with constant and varying loads, throttle pulsations, and scenarios both with and without gear shifts. To avoid instability during the real-world tests, the estimator was silenced while gear shifting was happening to overcome rapid changes in dynamics. In resulted, the mass estimation achieved a maximum error of 2.8% and a root-mean-square (RMS) error of 350 kg. , reducing the RMS error to 310 kg for mass estimation and 0.24 degrees for grade estimation. This study highlighted the effectiveness of RLS with multiple forgetting factors in providing accurate and robust mass and grade estimations under dynamic driving conditions.

Lin et al. [12] introduced a mass estimation technique for heavy-duty vehicles (HDVs) with RLS algorithm that at the same time estimates vehicle mass and system error in longitudinal dynamics. The research conducted in real-world scenarios on highways and through simulations a diesel-engine heavy-duty vehicle equipped with a 12-speed transmission is used. Three load conditions were implemented in the real-world tests: a completely loaded trailer (48 tons), an empty trailer (23.2 tons), and a trailer that was not present (9.5 tons). These conditions were designed to simulate typical driving scenarios, including acceleration, cruising, and stopping.

The system error, referred to as correlated noise, resulted in consistent variances due to factors such as sensor drift and external disturbances. The accuracy is optimized by 8.8% as a result of the mass estimation error being reduced from 16% to 7.2% through the integration of this system error into the model. The tests demonstrated optimal performance under maximum load conditions, exhibiting an average absolute inaccuracy of merely 4% of the entire load. This method illustrates the efficacy of integrating system error factors with RLS algorithms to improve mass estimate precision, rendering it particularly suitable for sophisticated vehicle control systems such as automated gear shifting and fuel-efficient cruise control.

1.2.2 Kalman Filters

Focusing on the accuracy and robustness of real-time applications, Lingman and Schmidtbauer [13] proposed a Kalman Filtering-based technique for the simultaneous estimation of vehicle mass and road slope in heavy-duty vehicles(trucks). Evaluation was performed on two different configurations: one that utilized speed measurements in conjunction with propulsion force data, and another that incorporated an accelerometer for the purpose of measuring specific forces. By utilizing multiple sensors, the second configuration enabled the separation of mass and slope estimation into independent filters, thereby eradicating the necessity for propulsion force models in slope estimation and enhancing performance. The results indicated that the use of multiple sensors substantially improved the accuracy and robustness of the system, particularly under varying road and noise conditions. Consequently, it was rendered suitable for real-time heavy-duty vehicle operations. Winstead and Kolmanovsky [14] introduced a technique for the simultaneous estimation of vehicle mass and road gradient utilizing an Extended Kalman Filter (EKF) in conjunction with Model Predictive Control (MPC). The EKF assessed road gradient and mass in real time, while MPC dynamically regulated engine torque to enhance parameter identifiability. The research concentrated on a mid-sized passenger vehicle (1500 kg) and verified the methodology using simulations, accounting for engine torque errors, road gradient fluctuations, and system noise.

The strategy tackled noisy situations resulting from uncertainties in engine torque output, road surface abnormalities, and sensor inaccuracies. It limited vehicle speed to 18.67–21.33 m/s and implemented probabilistic limitations to address these uncertainties. The results indicated a road grade estimation error of 0.5 degrees and a vehicle mass estimation error within 5%, illustrating the approach's durability and efficacy under severe dynamic settings.

A dynamic joint estimation technique for vehicle mass and road slope was introduced by Zhao et al. [1]. This technique is capable of managing the intricacies of braking and turning functions in real-world driving and typical traffic conditions.

The methodology employs an EKF for road slope estimate, utilizing a RLS algorithm with a forgetting factor for mass estimation. A nested loop framework is employed to accomplish this, which decouples the strong interdependence between mass and road slope. This ensures precise and independent estimations of the two parameters while minimizing error propagation between the two parameters. The

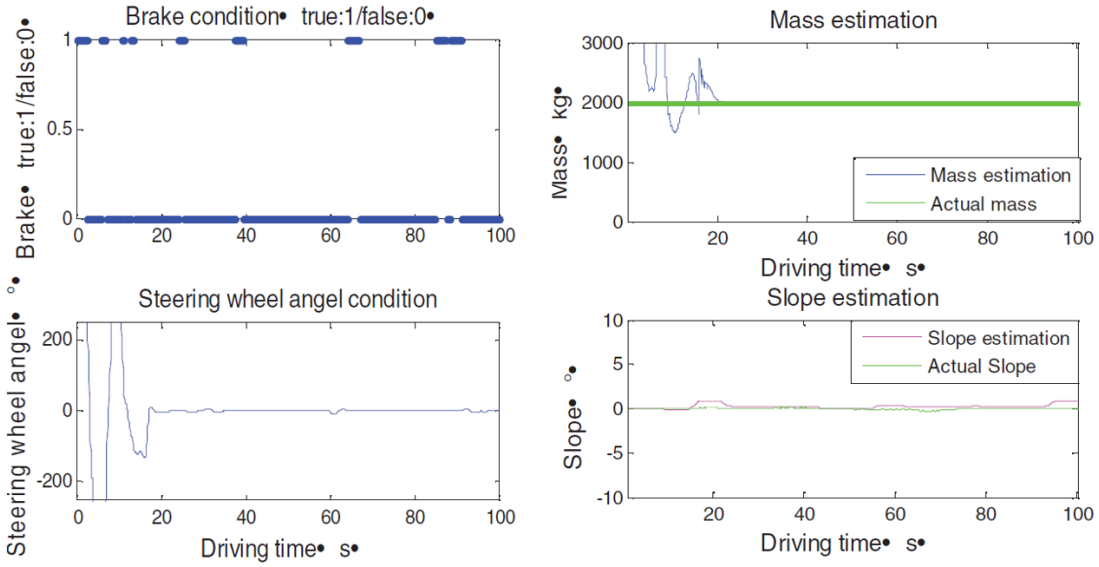

FIGURE 1.1: Small amount of brakes and turns, [1]

dynamic model's impacts of braking and turning are mitigated/eliminated by the integration of state maintenance and segment estimation in the approach in Fig. 1.1 and 1.2, eliminated Real-world experiments were conducted on a 2015 Ford Edge model vehicle in Chongqing, China, on flat terrain, including uphill and downhill periods. The vehicle was operated by passenger groups 3 and 5, with total weights of 2121 kg and 2211 kg, respectively. Mass estimation errors ranging from 25.17 to 40.51 kg, or 1.18% to 1.83% error, were observed in the results, indicating the algorithm's durability, precision, and adaptability to intricate driving scenarios.

Zhang et al. [15] proposed an alternative method for the real-time estimation of vehicle mass and road grade, which was evaluated on a 4WD electric minicar. The methodology developed by integrating data from many sensors relies on a Kalman Filter to calculate the road gradient, including data from wheel-based speed sensors, GPS, and INS to mitigate noise and drift. This approach

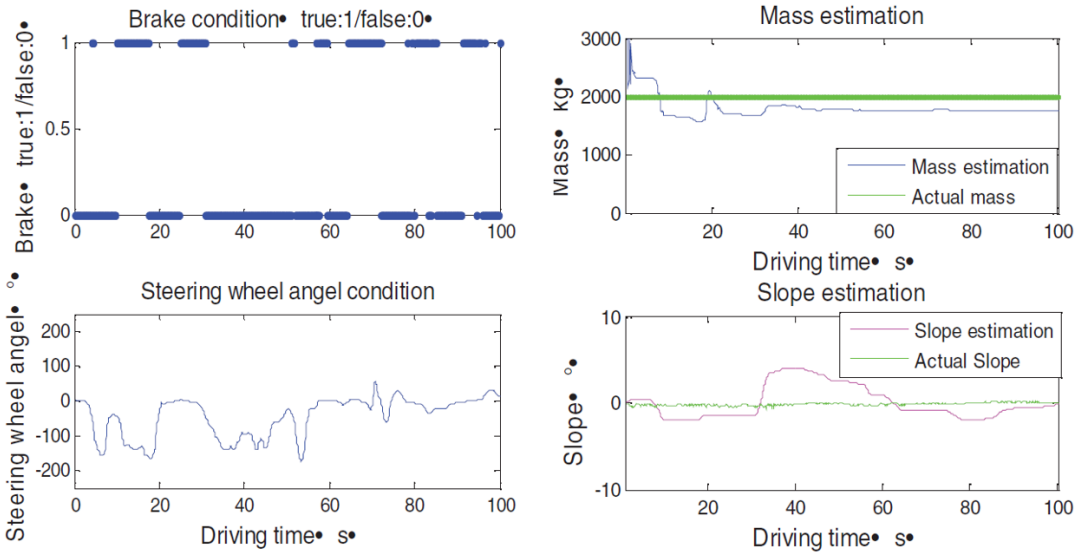

FIGURE 1.2: Lots of brakes and turns, [1]

yielded precise and accurate grade estimates. The RLS method was employed to improve accuracy and reduce variability in the prediction of vehicle mass. The mass estimation and road grade inaccuracies were within 5%, and the performance remained robust under dynamic conditions during real-world testing on diverse grades, validated using Hardware-in-Loop (Vector tool called CANoe).

1.2.3 Other Techniques

Mahyuddin et al. [2] suggested a sliding-mode term-based adaptive observer-based vehicle mass estimation technique for robustness and finite-time convergence. The approach included additional filtered parameters, a forgetting factor, and relied on Lyapunov Theory to ensure the stability and convergence of estimate errors. In order to replicate real-world conditions, tests were conducted on a small-scale vehicle (10 kg nominal mass) with step changes in mass (e.g., adding or eliminating weights of 1.85 kg). Noise and velocity variations were also applied. In Fig. 1.3 the algorithm's performance at a velocity demand of 0.14 m/s with introduced noise, wherein mass estimate precisely followed the actual values. Simulations additionally confirmed the algorithm's robustness. The research exhibited precise and swift mass estimate with negligible mistakes in dynamic and noisy conditions,

underscoring its applicability for real-time use in commercial vehicles such as buses functioning under diverse loads.

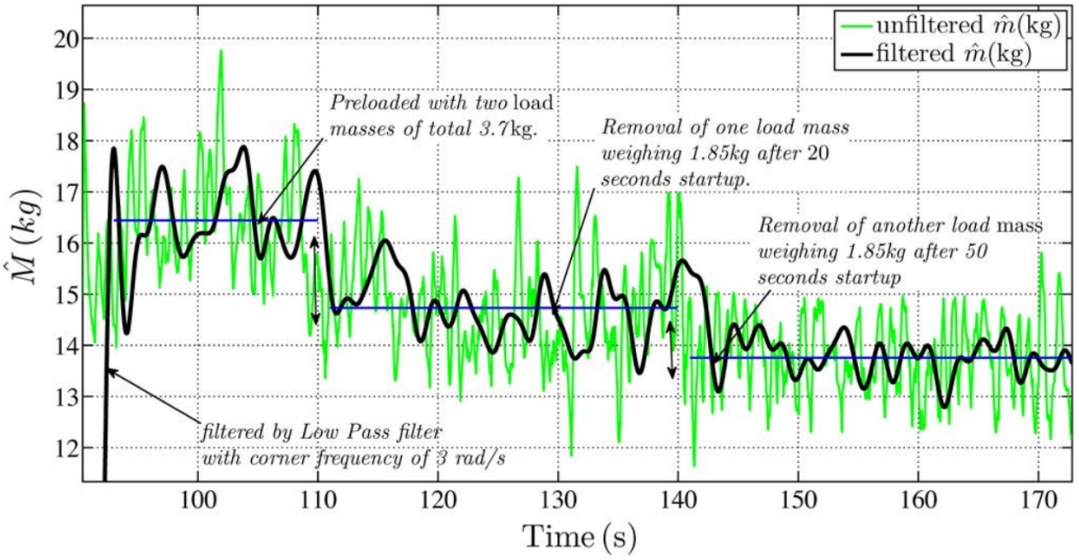

FIGURE 1.3: Mass estimation, $\hat{m}$ kg, [2]

DeBruyne et al. [16] introduced a novel algorithm for the online estimation of vehicle inertial parameters, such as mass, center of gravity (COG) position in the horizontal plane, and moments of inertia, with the objective of enhancing chassis control systems. The algorithm calculates total vehicle mass by analyzing suspension displacement signals and stiffness attributes, then allocates payload mass (passengers and luggage) across designated spots with a Monte Carlo method, which incorporates uncertainties via probabilistic modeling. Validation studies utilizing Kinematics and Compliance (K&C) data demonstrated good precision, with estimation errors for mass and other parameters often ranging from 1% to 2%. This work emphasizes the significance of dynamic mass and parameter estimation in improving the safety and control performance of vehicles.

Torabi et al. [17] and Korayem et al. [18] proposed sophisticated approaches for mass estimate in heavy-duty vehicles, applying machine learning and dynamic modeling techniques. A Feed Forward Neural Network (FFNN) was developed by Torabi et al. [17] to estimate vehicle mass and road grade by utilizing standard onboard signals, including speed, acceleration, and engine torque. The collection comprised six synthetic road segments, each measuring 10 kilometers, alongside

actual highway data from Sweden, with mass values ranging from 20 to 34 metric tons under various driving situations. The FFNN attained a 1% RMS error in mass estimate and 0.10–0.14 degrees in road grade, markedly surpassing conventional model-based approaches. Conventional methods, including recursive least squares and Kalman filtering, generally provide mass estimation inaccuracies of 2–7% and road grade inaccuracies of 0.2–0.77 degrees RMS.

Korayem et al. [18] suggested two methodologies for estimating trailer mass in tractor-trailer systems: a system model-based approach, which resulted in a maximum error of 12%, and a Deep Neural Network (DNN)-based technique, which attained a maximum error of 10%. The dataset included 50 simulated maneuvers and experimental data gathered from an electric Chevrolet Equinox towing a trailer, including diverse payloads, geometry, and road conditions. DNN demonstrated adaptability and cost-efficiency by generalizing effectively across various configurations without retraining.

Both investigations underscore the importance of machine learning in the creation of precise and resilient mass estimations. These technologies improve vehicle safety, stability, and control performance, providing effective solutions for commercial vehicles such as buses.

1.2.4 Contributions

Commercial passenger vehicles have to operate at different body weight conditions, since the number of passengers carried in these vehicles change frequently. Such mid-operation changes in the inertia of the vehicle affect the fuel efficiency significantly, making online gross-weight estimation necessary. Our survey on the relevant literature indicates the existence of various methods with different levels of computational power and sensing hardware requirements. Some of the most advanced methods involve the use of neural networks that need to run continuously, or additional sensors that would not be otherwise needed in commercial vehicles. While the accuracy of such algorithms are exceptionally high, they are

not cost-efficient. This is an important concern for commercial vehicles that are usually planned for mass production.

Classical prediction-error-based online estimation methods, on the other hand, offer a cost-effective alternative; since they do not require specialized equipment capable of running complex computations, or additional sensors just for mass estimation. In return, making accurate and reliable predictions require an accurate system model, including the road conditions such as the inclination angle. These methods have been tested in many different vehicle types, road conditions and driving configurations. Our survey indicates that the success of these methods depend largely on these conditions, and there is no clear indication for the superiority of a particular approach.

This study investigates the efficacy of four different estimation-error-based vehicle mass estimators under the road and driving conditions typical for electric commercial passenger vehicles that are driven in city traffic. Our analysis reveals whether the use of classical and cost effective approaches in our particular application scenario yield an acceptable estimation accuracy, and if so the conditions that enable the satisfactory performance. The outcomes of this study are expected to illuminate key modeling aspects that could affect the estimation accuracy significantly, and the driving conditions under which the investigated methods are prone to fail.

Chapter 2

Experimental Setup

2.1 Development of the Test Vehicle

This study utilized the JEST Electric Vehicle, a 12-passenger electric commercial vehicle developed and manufactured by KARSAN Automotive [19] in Bursa. The vehicle is primarily distributed in the North American, Japanese and EU markets. An outdated test vehicle was revitalized to advance autonomous vehicle research. The electronic and mechanical systems of the vehicle were significantly upgraded during this process, resulting in a configuration that closely resembles a newly manufactured model. Initially designed for the North American market, the vehicle was modified to meet the requirements of the EU market.

The physical dimensions of the test vehicle are 5845 mm in length, 2520 mm in width, and 2850 mm in height. A maximum range of 210 km is possible per charge, as it is endowed with a usable battery capacity of 75.8 kWh. For this study, only the conventional systems of the JEST EV model were utilized, without incorporating additional components, despite the vehicle's capability of supporting advanced sensors and processors for autonomous operation. This approach was adopted to ensure the generalization of the results to analogous vehicle models.

The JEST EV has a lightweight chassis engineered for energy economy and an advanced battery management system designed to monitor and control power consumption. Furthermore, regenerative braking technology improves the range of the vehicle by converting kinetic energy into stored energy during deceleration. The following sections provide a detailed analysis of the vehicle and the components employed in this research.

FIGURE 2.1: Jest EV Lansman Photo, 2019

FIGURE 2.2: Vertical Forces on The Vehicle are in Equilibrium

TABLE 2.1: Tire Based Weight Distribution and Wheelbase

Definition	**Value**	**Unit**
P_1&P_2	1860	kg
P_3&P_4	1840	kg
L	3750	mm
P_{total}	3700	kg

2.1.1 Renewal Process

The vehicle, which was delivered in November 2023, underwent a comprehensive renovation as part of the project. The vehicle was prepared for testing over a period of approximately five months. During this process, all existing wiring was removed and replaced with around 3000 meters of new wiring to accommodate the upgraded components and systems. The vehicle underwent a comprehensive

transformation during this period, resulting in the fully equipped condition shown in Fig. 2.3, tailored to meet the specific requirements of our experiments.

2.1.1.1 Reception and Initial Assessment of Vehicles

A preliminary evaluation was conducted upon the vehicle's arrival to assess its existing condition and suitability for the project requirements.

Existing Wiring Evaluation: An assessment was conducted in collaboration with the prototype workshop and the engineering department to ascertain the effect of the antiquated wiring system on the vehicle's safety and performance. An examination was conducted to determine the necessity of replacing the obsolete and deteriorated wiring, which was incompatible with modern software and vehicle systems. Electrical systems required to meet the specifications of the current vehicle model were subsequently identified and procured.

Evaluation of Electronic Control Units (ECUs): The control specifications of the existing electronic control units were analyzed. The vehicle, having been inactive prior to the project, had most of its components removed for use in other vehicles and was delivered without any electronic control equipment. This necessitated the acquisition and integration of new ECUs to meet the project's requirements.

Trim and Door Components: As depicted in Fig. 2.3, unlike the wiring and control units, the vehicle was delivered with most interior components missing, except for the exterior trim elements. Critical components, including the dashboard, steering wheel, command/control systems, and the Human-Machine Interface (HMI) such as the touch screen, were absent. These components had to be replaced and installed to ensure the vehicle's functionality and alignment with the experimental objectives.

2.1.1.2 Replacement of Obsolete Wiring and Transformation of Vehicle Platforms

The vehicle's reliability and safety were improved by replacing its original wiring with robust layout. During this process, the vehicle, which was initially designed for an alternative market, was modified to comply with European standards through chassis modifications, thereby enhancing its compatibility with autonomous driving infrastructure.

Furthermore, the charging system and its components, which were initially situated at the front of the vehicle to comply with North American standards, were relocated and redesigned to satisfy the requirements of the European market. The body and chassis were restructured to support a 22 kW AC charging system, replacing the previous 7 kW AC system, thereby enhancing charging efficiency and market suitability.

2.1.1.3 Installation of New Wiring

Approximately 3 kilometers of new wiring were placed throughout the car. In accordance with modifications to the high-voltage management system, cable types and connection points were redefined to guarantee the safety of the electrical circuits and fulfill the criteria of the autonomous project. To improve safety, the electrical layout strategically positions cables at a safe distance away from critical components. Additionally, the risk of short circuits was mitigated by maintaining a minimum distance between power and data cables.

Tests were carried out on the connections pin-to-pin technic to guarantee their structural integrity and current-carrying capacity following the installation. Furthermore, the vehicle's The Controller Area Network (CAN) connections were meticulously assessed to ensure that the data exchange was uninterrupted

2.1.1.4 Renewal of Control Units

Selection and Installation of Control Units: The vehicle body was modified to comply with the requirements of the EU region, and electronic components that were specifically designed for this market were selected and installed. This phase guaranteed that the configuration was compatible with the most recent modification and that it complied with the regional norms.

Calibration and System Integration: Calibration procedures and software updates for each control unit were performed individually to activate the ECUs and bring the vehicle into operational state. Following this, functional tests were implemented to confirm the integrity of the system. During this process, necessary optimizations were implemented to enhance data collection sensitivity. In addition, the compliance of the pre-test control units with the project requirements was thoroughly evaluated and confirmed.

2.1.1.5 Final Inspections and Tests

Deployment Tests: The compatibility between the control units and the new installation has been tested. During these tests, the accuracy and timing of the data collected through each control unit were evaluated by checking the communication lines. In addition, 1,000 km road and function tests have also been conducted.

Data Collection and Monitoring Tests: The tool has undergone data collection tests under conditions close to real test scenarios. Especially, it has been confirmed that the transactions were carried out without any interruption or deviation in the data flow.

FIGURE 2.3: Vehicle Before and After Renewal Process

2.1.2 Vehicle Communication and High Voltage Network

The Controller Area Network (CAN) bus is a communication protocol that facilitates the transmission of data between ECUs in vehicles. The CAN bus, characterized by its cost-effectiveness and durability, facilitates real-time data sharing among many components, including the engine, gearbox, brake system, and air conditioning within the vehicle. Rather than relying on a central control unit, each ECU transmits its information across the network and acquires the necessary data. This system enhances vehicle efficiency and facilitates fault identification. In contemporary automobiles, there are numerous applications, with system-based or regional CAN BUS lines being the most prevalent. Data was gathered only from two of the five CAN Bus lines in our experiment vehicle while we were performing tasks on it. The visual representation of the general structure is depicted in Fig. 2.4.

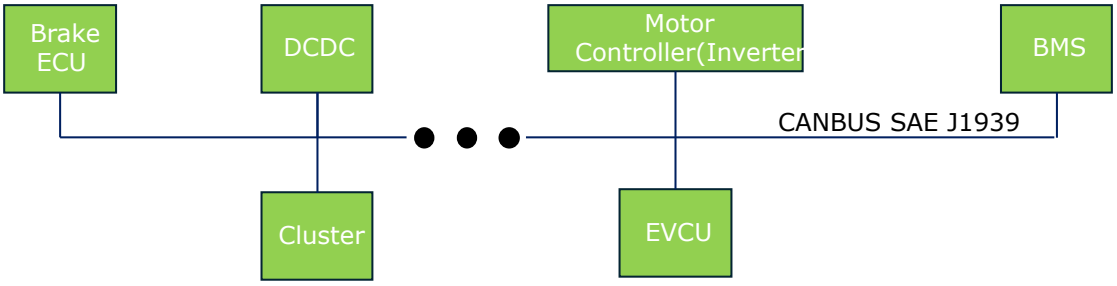

FIGURE 2.4: Vehicle Communication Topology

In electric vehicles, high-voltage (due to regulations and standards, high-voltage cables are manufactured in orange to ensure visibility and compliance with safety requirements) cables deliver electricity to the primary system, generally between 400V and 800V. These wires provide energy transfer from the battery to the electric motor, inverter, charging system, and other high-power subsystems, while also receiving energy during charging and braking. High-voltage systems are continuously monitored with specialized sensors and a High Voltage Interlock (HVIL) system, which can shut the system upon detecting a warning to ensure operational safety.

The secure and efficient transmission of high voltage is crucial for the operation and safety of electric cars. Figure 2.5 illustrates the appropriate energy distribution of the system. Electrical energy is converted into mechanical energy, which generates the traction force necessary to propel the vehicle.

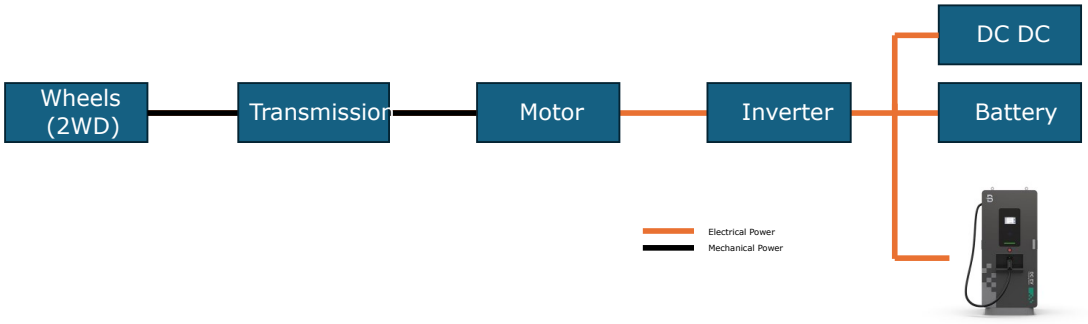

FIGURE 2.5: Vehicle High Voltage Topology

2.1.3 Related Electronic Systems

2.1.3.1 Electric Vehicle Control Unit

The Electrical Vehicle Control Unit (EVCU) is a software-based system that is primarily responsible for the control and supervision of the high-voltage (HV) systems of electric vehicles (component may be referred to by different names by other OEMs), unit and developed in the SIMULINK framework, is intended to enhance vehicle performance and ensure safe transportation. Its function is

especially crucial, as it supervises and regulates essential processes including motor control, regenerative braking, battery management, and power distribution.

Future research could involve the integration of the proposed algorithms into the EVCU, which would facilitate the real-time calculation of vehicle weight and road grade information for all vehicles that are to be manufactured.

2.1.3.2 E-Motor and Inverter

The traction management of electric vehicles are profoundly influenced by the integration of motors with inverters. The inverter plays a pivotal role by converting the direct current (DC) from the battery into alternating current (AC), enabling the motor to operate in Fig. 2.6. This conversion allows precise regulation of the motor's speed and torque, optimizing energy utilization and ensuring optimal driving performance under predefined limits at desired values.

Moreover, the inverter exchange critical data with the EVCU, including motor RPM, motor voltage, current, available torque, instantaneous torque, required torque and other parameters, via the CAN Bus at variable cycle intervals. This exchange of data provides real-time monitoring and control, which enhances the efficiency and safety of the electric vehicle during operation.

TABLE 2.2: E-Motor Specifications, [3]

Parameters	Value
Maximum Peak Output Power:	42.2 kWh
Maximal Torque:	37,9 kWh (90 %)
Continuous Power	352 V
Battery weight:	278 kg
Battery energy density:	152 Wh/kg
Speed range:	96 (96s1p)

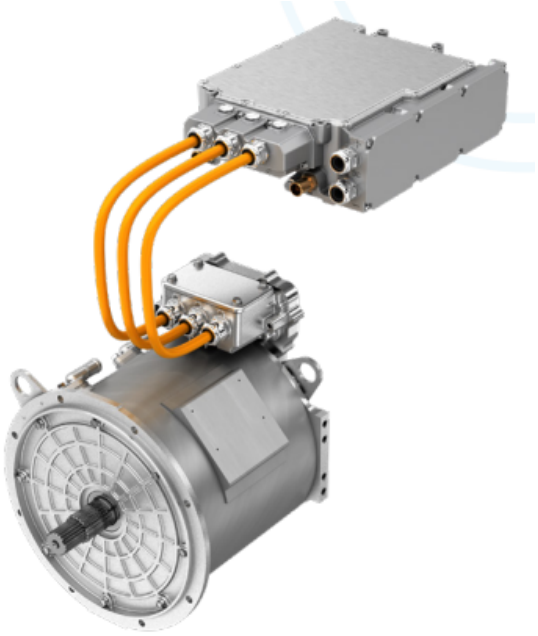

FIGURE 2.6: E-Motor and Inverter, [3]

2.1.3.3 Battery

Electric Vehicle battery refers to high-capacity energy storage systems (ESS) which are utilized as only power sources for electric vehicles. Nickel (Ni), Manganese (Mn), and Cobalt (Co) are the three elements that make the NMC-type lithium-ion batteries that are being utilized in the battery of our test vehicle. Nevertheless, electric vehicles employ a variety of battery chemistries, including Lithium Iron Phosphate (LFP) and Lithium Nickel Cobalt Aluminum Oxide (NCA).

Battery Management System (BMS) is technology in battery systems to supervise critical metrics, including temperature, current and voltage, throughout every

Table 2.3: Battery Specifications, [4]

Parameters	Value
Total battery capacity:	42.2 kWh
Usable battery capacity:	37,9 kWh (90 %)
Nominal Voltage:	352 V
Battery weight:	278 kg
Battery energy density:	152 Wh/kg
Cells:	96 (96s1p)
Cell:	Samsung SDI
	120Ah prismatic NCM 622
	200Wh/kg
	Active refrigerant cooling

battery pack, module and cells. This monitoring improves safety and maximizes the battery's longevity by ensuring the system functions within secure and efficient parameters. Furthermore, it manages charge, discharge and fail-safe functions. The BMS processes battery data to enhance the efficient use of multiple battery configurations.

Each BMW NMC battery has a capacity of 42.2 kWh, and the test vehicle in this study is equipped with two of these batteries. The comprehensive specs of these batteries are presented in Tab. 2.3 for reference.

Figure 2.7: BMW I3 Battery Pack, [4]

2.1.3.4 Brake System

The braking system of a vehicle is a critical component for decelerating, stopping, or controlling the vehicle's speed by reducing its kinetic energy during motion. It ensures safe and controlled operation with the driver's commands. However, advancement on modern technology, it possible for advanced driver assistance systems (ADAS) to partially or entirely can be manage braking systems.

The regenerative and service brakes are simultaneously activated by the brake pedal in the test vehicle, which initiates the braking system. Notably, the regenerative braking system is rendered unavailable at velocities below 5 km/h. Additionally, the vehicle can decelerate without engaging the service brake by activating regenerative braking upon the release of the accelerator lever. This procedure recharges the battery during deceleration, which not only reduces the vehicle's speed but also helps in energy recovery.

Regenerative Brake: Electric and hybrid vehicles utilize regenerative braking, an electronic system that converts the vehicle's kinetic energy (AC) into electrical energy during deceleration, subsequently charging the battery (DC) via an inverter. As the vehicle slows down, the electric motor operates as a generator, converting the wheels' kinetic energy into electrical energy. The battery accumulates energy, hence extending the vehicle's range.

Regenerative braking improves energy efficiency and reduces stress on the braking system, therefore extending the longevity of the brake pads. We employed this feature for deceleration during our study, enabling us to reduce our vehicle's speed.

Hydraulic/Service Brake System: The hydraulic brake system utilizes hydraulic pressure to execute the braking operation in cars. The master cylinder produces hydraulic fluid pressure upon depressing the brake pedal, which then travels to the brake calipers or wheel cylinders through the brake lines. Brake pads or brake shoes decelerate or halt the vehicle by engaging with the disc or

drum surface. The sensors positioned on each wheel refresh the wheel speeds every 20 milliseconds and transmit them to the CAN bus. Furthermore, it supplies the vertical and lateral acceleration data that are crucial for our research.

2.1.3.5 Additional Systems

Cluster: The vehicle cluster functions on the dashboard, allowing the driver to monitor essential information regarding the vehicle. These are speed, RPM, battery level, and engine temperature, as well as warning lights and indications related to electrical systems. It can be either digital or analog and may also have other capabilities, like navigation and entertainment, in modern vehicles. The cluster enhances safety by allowing the driver to rapidly access critical information/warnings while driving.

DC-DC Converter: The DC-DC converter is a power electronics device that is intended to facilitate the conversion of energy between with varying voltage levels in electric vehicles. It enables the transmission of electricity from a high-voltage source (nominal battery voltage level 350V) to low-voltage systems(12-24V), including automobile electronics and auxiliary accessories. Before the activation of the DC-DC converter and the HV system, certain components are powered directly by the 12V battery in our case. Once the DC-DC converter is operative, it provides power to the 12V battery and the low-voltage systems, thereby supports the electronic components and accessories of the vehicle to operate consistently and uninterrupted.

2.2 Vehicle Longitudinal Dynamics

Longitudinal vehicle dynamics is a field that analyzes the forces governing and affecting a vehicle's motion in both forward and reverse orientations. Vehicle performance includes acceleration, breaking and traction. In this study, based on Newton's second law of motion, equations are derived Eqn. 2.1, the variables F_{trac},

F_{aero}, F_{roll}, and F_{grade} denote the traction force, aerodynamic drag force, rolling friction force, and the uphill driving force, respectively [20].

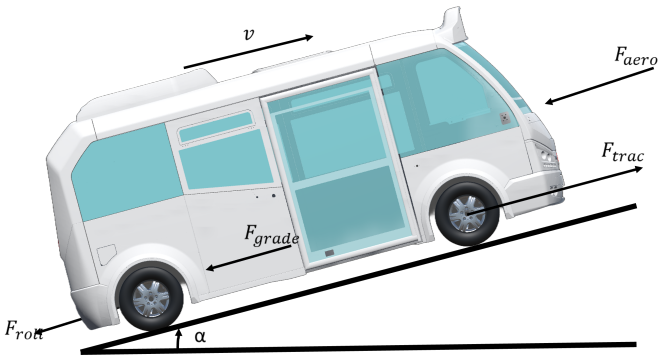

FIGURE 2.8: Forces acting on the vehicle

$$F_{traction} - m \cdot a_x = F_{roll} + F_{grade} + F_{aero} \tag{2.1}$$

m: Vehicle Mass

a_x: Longitudinal acceleration

F_{aero}: Aerodynamic Drag Force

F_{roll}: Rolling resistance

F_{grade}: Road grade

$F_{traction}$: Longitudinal force acting on the vehicle

2.2.1 Rolling Resistance

Rolling resistance is the frictional force resulting from the relationship between the road surface and wheels [20].

$$F_{roll} = f_r \cdot m \cdot g \tag{2.2}$$

f_r: Rolling resistance coefficient (Considered as a linear function of speed), [21]

m: Vehicle mass g: Gravitational acceleration (9.81 m/s^2)

$$f_r = 0.01 \cdot \left(1 + \frac{V}{160}\right) \tag{2.3}$$

V: Vehicle Speed

2.2.2 Aerodynamic Drag, Air Resistance

Aerodynamic drag is the resistance generated by a moving vehicle when it interacts with the air. The factors influencing this resistance include aerodynamic design, velocity, vehicle surface area, and air density [20].

$$F_{aero} = \frac{1}{2} \cdot p \cdot A_f \cdot C_d \cdot V_{rel}^2 \tag{2.4}$$

p: Air density

A_f: Vehicle frontal area

C_d: Dimensionless drag coefficient

V_{rel}: Vehicle relative speed to the air

FIGURE 2.9: Front View of Jest EV

2.2.3 Grade Resistance

Grade resistance refers to the gravitational force experienced by a vehicle when driving inclines or declines. During ascension, gravity hinders movement, requiring increased power output from the engine. Conversely, during descent, gravitational forces accelerate the vehicle, requiring increased braking efforts. This force varies according to the angle of inclination and the mass of the vehicle [20].

$$F_{grade} = m \cdot g.sin(\theta) \tag{2.5}$$

θ: Road grade

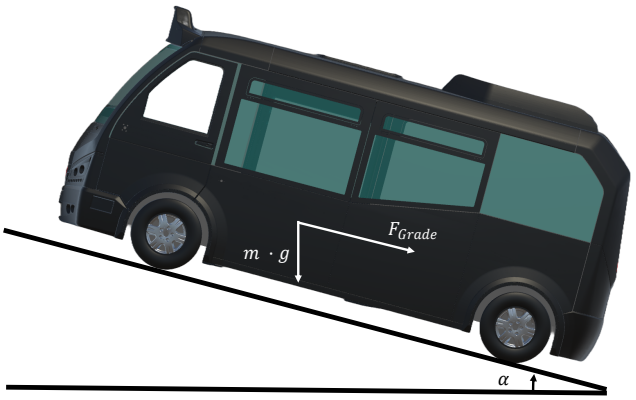

FIGURE 2.10: Grade Resistance Acting on The Vehicle

2.3 Measured Signals

The structured communication format of the CAN Bus SAE (Society of Automotive Engineers) J1939 protocol, developed by Bosch in 1986 [22], which is specifically designed for data transmission in heavy-duty vehicles such as trucks, buses, and agricultural equipment, consists of a multitude of messages. These messages are classified according to the information and metrics transmitted from various vehicle components, including engine speed, ambient air temperature, battery voltage, and current, as denoted by a Parameter Group Number (PGN), using a 29-bit

identifier. In addition, the priority field of the 29-bit identifier is included to establish the urgency of each message. Messages with higher priority are prioritized on the network. Followed by the actual information, raw data encapsulated in an 8-byte section. In total, with other sections, a standard CAN message and an extended CAN message consist of 96 bits and 114 bits, respectively.

Interpreting these communications can be difficult, since the data is typically presented in raw form. To address this, CAN Database Container (DBC) files are used as decoders , enabling the structured interpretation of the 8-byte data section. These files facilitate a comprehensive understanding of the meaning, relevance and structure of the data embedded within the J1939 messages, significantly enhancing the analysis and usability of vehicle data. For this study, we developed our own DBC file in Fig. 2.12, which allowed us to filter hundreds of messages and access the raw data efficiently.

TABLE 2.4: Message List

List of Messages		**Cycle Time of The Messages**
Wheel Based Speed	km/h	20 ms
Motor Torque	N	10 ms
Requested Torque	N	100 ms
Vehicle Speed	km/h	100 ms
Steer Angle	rad	100 ms
Lateral Acceleration	m/s^2	100 ms
Longitudinal Accelerations	m/s^2	100 ms

2.3.1 Data Extraction from Vehicle Communication Network

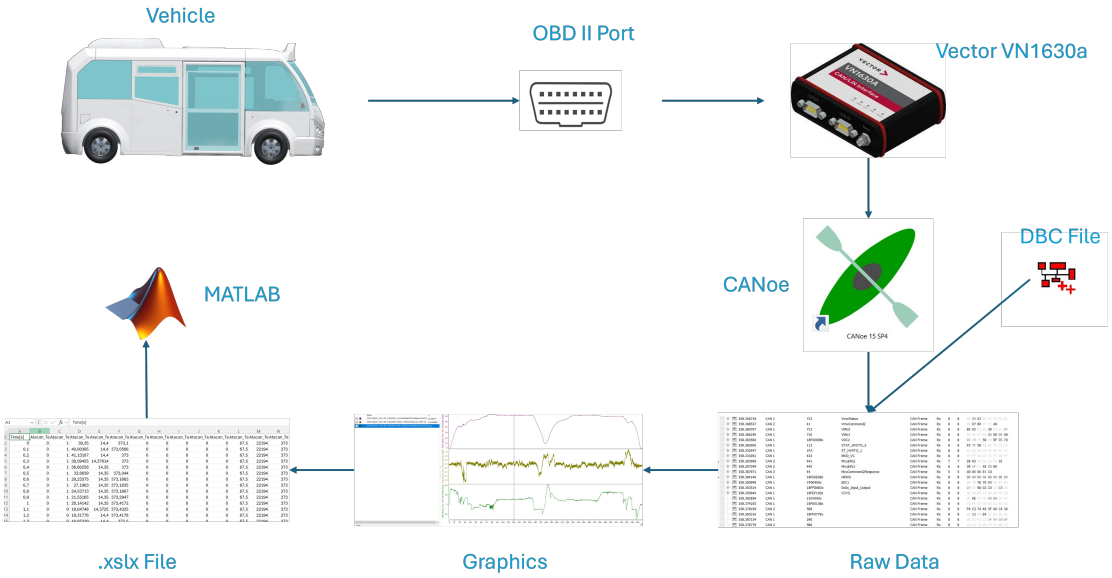

FIGURE 2.11: Data Extraction Process

The performance data of the electric vehicle used in the experimental studies was collected via the vehicle's CAN Bus. In this study, parameters such as motor torque, speed, acceleration, high voltage data, and energy consumption from the critical systems of the test vehicle were obtained through CAN Bus. To record data, a Vector VN1630a data logging device compatible with the vehicle's CAN bus was connected to the OBD2 port, enabling access to the vehicle's communication network. This device records messages on the CAN Bus at designated intervals, providing the necessary infrastructure for data analysis. The logging device connects directly to the CAN Bus, collecting each message and parameter in real time, and transfers this data to the CANoe program on a computer. During testing, we can monitor the data live and visually track parameters such as torque, speed, and acceleration through a graphical interface. This was particularly useful for observing changes in these parameters on inclined sections. Subsequently, the raw data collected was interpreted using a customs dbc file specifically prepared for our study. Through the same program, the data was categorized in milliseconds and exported in .csv format for the analysis.

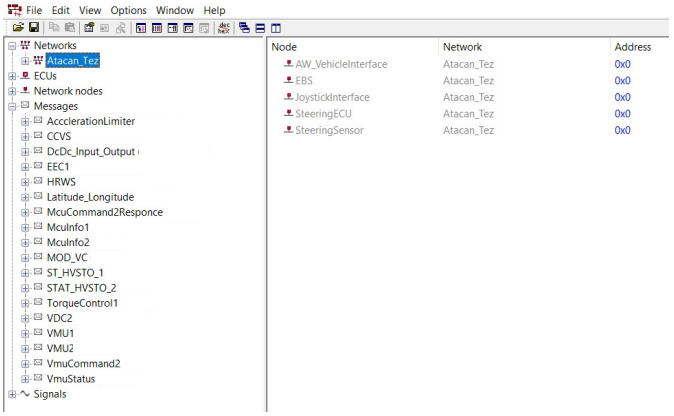

FIGURE 2.12: Interface of DBC File

2.4 Configurations of the Test Tracks and Driving Settings

The experiments were conducted on two distinct tracks in Bursa, involving a total of five cases performed under varying scenarios. Track 1, a controlled and relatively low traffic area parallel to the highway in Fig. 2.14, while Track 2 was on a road with significantly higher traffic levels compared to the first track in Fig. 2.19.

2.4.1 Description of Track 1

Track 1 is approximately 5 km long with an ascent and descent of 47 meters depicted in Fig. 2.13. During the tests, the route was completed by returning in the same direction to end parallel to the starting point Fig. 2.15. Throughout the tests, the average maximum air temperature was around 28°C, and the humidity level was approximately 40%.

TABLE 2.5: Path Specifications of Track 1

Parameters	**Value**	**Unit**
Distance	5108	m
Lowest Point	61	m (at 3.69km)
Highest Point	108	m (at 2.25km)
Uphill	29221	km (35.2%)
Downhill	29221	km (35.2%)
Flat	16072	km (28.2%)
Height Gain	47	m

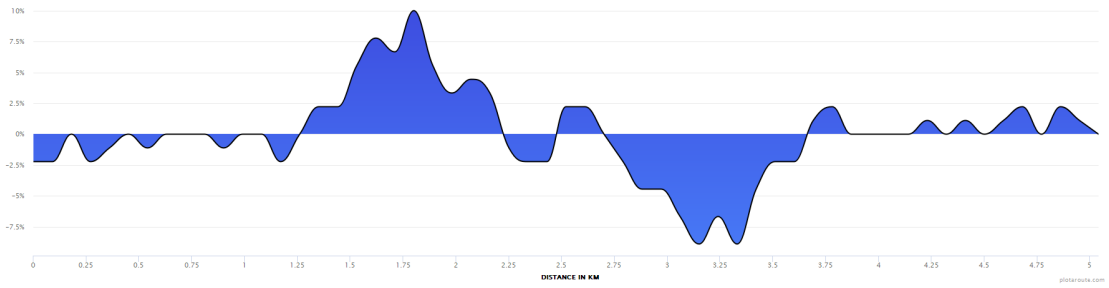

FIGURE 2.13: Track 1 Route Elevation Profile [5]

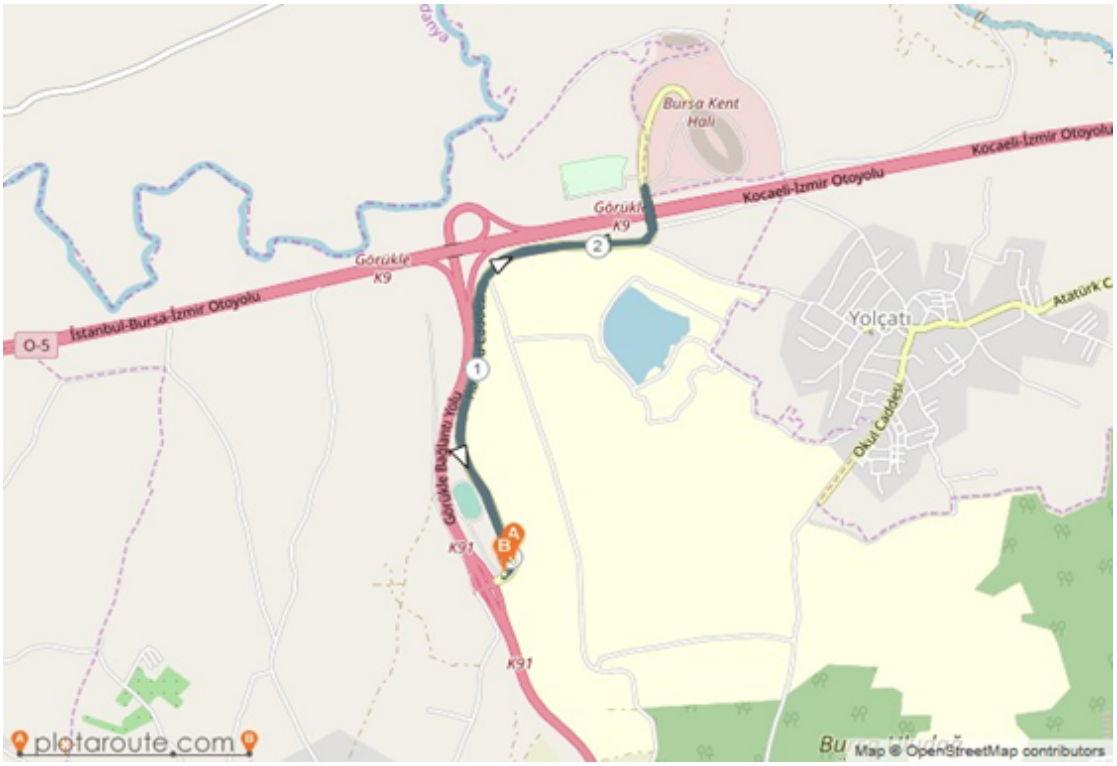

FIGURE 2.14: Track 1 Route on the Map, [5]

FIGURE 2.15: The Starting Point for All Tests Conducted in Case 1

General Characteristics of the Track

• **Length and Surface Types:** The section of the road where data was collected is 5,108 meters long. It is a divided, dual-lane asphalt road primarily used by trucks heading to the Bursa Fruit and Vegetable Market, leading to occasional depressions in the road surface.

• **Inclined Sections:** Certain parts of the track have specific inclines in Fig. 2.17. These inclined sections allowed for the analysis of key parameters such as motor power-torque, braking performance (regeneration), acceleration and road grade effect in various uphill and downhill scenarios.

• **Road Curves:** The track's sharp and wide turns on the track, in Fig. 2.14 and 2.17 , allowed us to observe the impact of these maneuvers on the vehicle's

dynamics, particularly on torque and vehicle inertia.

• **For the Live Map:** [23]

2.4.1.1 Case 1

The test scenarios, in Case 1, were carried out with four different total vehicle weights and carried out by the same driver. The total vehicle masses were measured with a precision scale and adjusted according to the predetermined weight. In Test 1, the vehicle's curb weight of 3700 kg, without any additional mass. The base and additional weight information for the other tests are provided in Table 2.6.

TABLE 2.6: The tests and vehicle weights for Case 1.

Case	Test	Weight of The Vehicle	Additional Weight Driver/Co-pilot etc.	Total Weigt of The Vehicle
1	1	3700 kg	210 kg	3910 kg
	2	4200 kg	115 kg	4315 kg
	3	4600 kg	210 kg	4810 kg
	4	5000 kg	210 kg	5210 kg

Note: Driving was performed with consideration for factors such as acceleration, break distance, and skidding relative to vehicle weight. Although all drives were performed by the same individual, the vehicle data exhibited variations due to dynamic and environmental factors.

• **Test 1:** Conducted using the vehicle's baseline weight, defined as the unloaded curb weight.

• **Tests 2, 3 and 4:** The vehicle weight gradually increased, and the tests were carried out according to the specified weights, as shown in Tab. 2.6, including the driver. In addition tools and, in some cases, the added weight of an additional colleague who participated in the tests (Tests 1, 3, and 4).

• **Weight Adjustment:** Before each test scenario, the vehicle's weight was adjusted to match the predetermined target weights by loading sandbags, measured

using a scale.

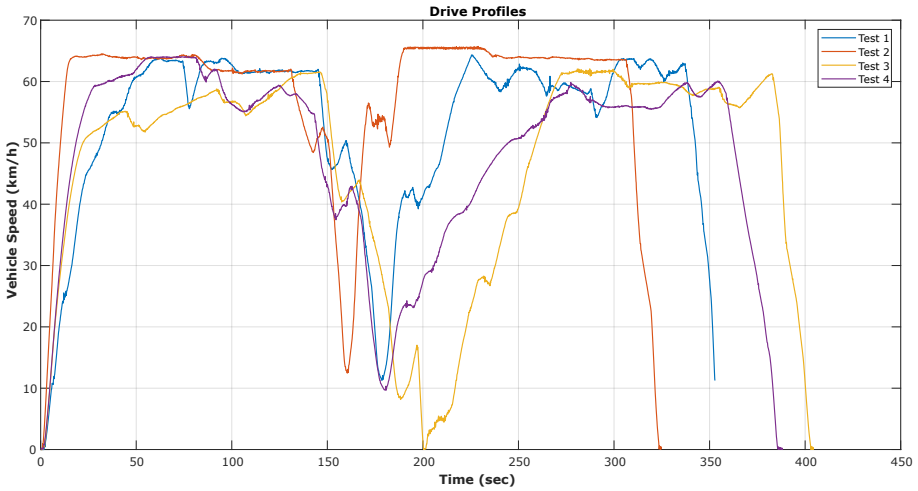

FIGURE 2.16: Case 1, Drive Profiles

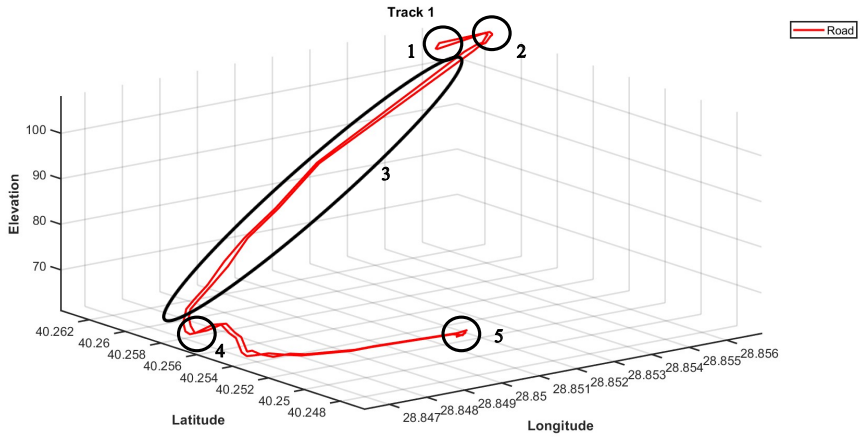

FIGURE 2.17: Track 1 in 3D view. Section 1: U-Turn, Section 2&4: Curve, Section 3: High-inclination, Section 5: Start-Finish Point

Speed profiles of the case 1's test over time at certain vehicle mass are shown in Fig. 2.17, which provides important information about how these variables interact during testing. The data indicates that the heaviest vehicle does not invariably correlate with the longest track completion time, nor does the lightest vehicle constantly attain the maximum speed. The complexity of the factors that influence vehicle performance is underscored, as weight alone is not enough to predict outcomes such as speed or completion time.

Although the tests were administered by the same driver to ensure consistency, environmental influences seem to significantly influence the outcomes. Vehicle dynamics and driver performance may be influenced by factors such as resistance forces, road conditions and temperature. Moreover, fluctuations in vehicle weight, maybe resulting from load distribution or payload modifications, may affect handling and acceleration attributes. The driver's psychological condition, encompassing weariness, concentration, and decision-making in test scenarios, is identified as a crucial determinant.

As illustrated in Fig. 2.16, which gives critical information. The data indicates the heaviest vehicle does not always correspond with the longest test completion time, nor does the lightest vehicle always achieve the highest speed. The intricacy of the elements affecting vehicle performance is emphasized, as weight alone cannot adequately forecast variables such as velocity or duration of completion.

2.4.1.2 Case 2

Case 2 is a driving scenario in which the start and end points of the Case1 are chanced in the same track. It starts and ends at B point in Fig. 2.18 This case is conducted to evaluate the vehicle's limits in inclined and curvy sections and to enable us comparison estimation algorithms performance with Case 1. The vehicle weight information is provided in Tab. 2.7.

Table 2.7: The test and vehicle weight for Case 2.

Case	Test	Weight of The Vehicle	Additional Weight Driver/Co-pilot etc.	Total Weigt of The Vehicle
2	**5**	**3700 kg**	**210 kg**	**3910 kg**

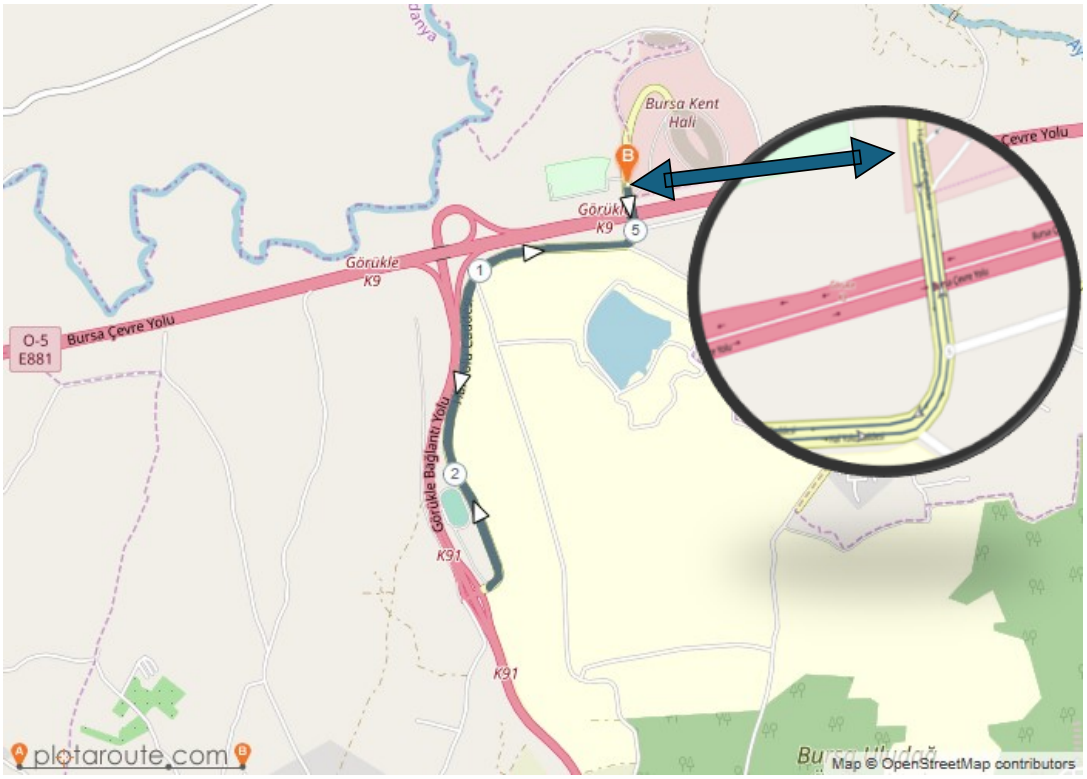

FIGURE 2.18: Case 2 Route on the Map, [5]

2.4.2 Description of Track 2

A nearly flat route, 10 kilometers in length, was chosen to conduct Case 3, 4 and 5 under three distinct scenarios based on route length, road conditions and driving style. In the first scenario, data were collected during normal driving within flowing traffic, which included navigating a route with traffic lights.

• **Length and surface types:** The section of the road where data were collected is 10.287 km (case 3) and 2.362 km (case 4-5) km meters long. It is a divided, dual-lane road and connects a residential area, a heavy industrial zone, and central hospital in Bursa. Case 4 and 5 are part of this route from the same starting point, as shown in Fig. 2.19 with a length of 2.362 km long, without any U-turn and traffic lights.

• **Inclined sections:** A nearly flat road with an elevation difference of 6 meters for all three cases.

TABLE 2.8: Path Specifications of Track 2

Parameters	Value	Unit
Distance	10287	m
Lowest Point	62	m (at 0.54km)
Highest Point	68	m (at 0.00km)
Uphill	3.42	km (33.2%)
Downhill	3.33	km (32.4%)
Flat	3.51	km (34.1%)
Height Gain	6	m

• **Road curves and traffic lights:** The route, which can be characterized largely as predominantly flat, involves a U-turn at a junction mid-way, with the recording concluding parallel to the starting point. Furthermore, the route includes four traffic lights, introducing acceleration, deceleration and interruptions to the driving flow only for case 3.

• **For the Live Map:** [24]

FIGURE 2.19: Track 2 Route on the Map

2.4.2.1 Case 3

The driving profile for Case 3, Test 6, conducted in normal traffic with a vehicle weight of 3700 kg. As shown in Fig. 2.20, the vehicle came to a complete stop at three of the four traffic lights along the route, with the vehicle speed dropping to 0 km/h. This case allowed us to test a scenario with minimal-grade effects.

TABLE 2.9: The test and vehicle weight for Case 3.

Case	Test	Weight of The Vehicle	Additional Weight Driver/Co-pilot etc.	Total Weigt of The Vehicle
3	**6**	**3700 kg**	**210 kg**	**3910 kg**

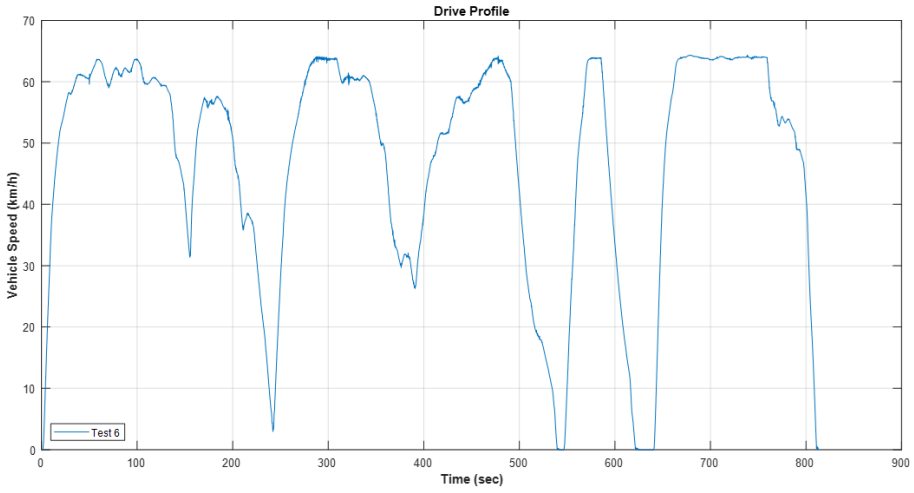

FIGURE 2.20: Case 3, Drive Profile

2.4.2.2 Case 4 & 5

The vehicle weight for Case 4 and Case 5 was 3700 kg, and both tests were conducted on Track 2. Similarly to Case 3, the tests started at the same point and ended at the target point after 2.362 meters, without encountering any traffic lights or decelerations apart from the final stop. Test 7 utilized an aggressive driving technique, while Test 8 adopted a pleasant driving method. Consequently, as demonstrated in Fig. 2.21, Case 5 required an additional 13 seconds to complete compared to Case 4.

TABLE 2.10: The tests and vehicle weights for Case 4 & 5.

Case	Test	Weight of The Vehicle	Additional Weight Driver/Co-pilot etc.	Total Weigt of The Vehicle
4	**7**	**3700 kg**	**210 kg**	**3910 kg**
5	**8**	**3700 kg**	**210 kg**	**3910 kg**

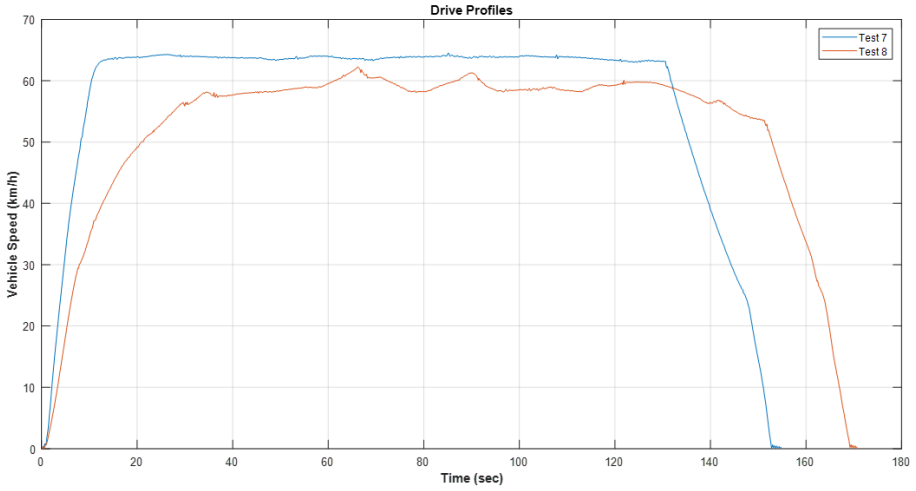

FIGURE 2.21: Case 4 & 5, Drive Profiles

Chapter 3

Methods for Model Identification and Online Estimation

3.1 Pre-Processing the Measured Data

3.1.1 Filtering Techniques and Their Implementation

In this study, we applied a low-pass filter to the measured signals as the time derivatives of the signals were calculated. The actual signal is first passed through the filter, and then the derivative is taken.

When taking the derivative of a signal in the discrete domain, high-frequency noise tends to amplify. That's why we observed an increase in spikes when applying an unfiltered derivative to the recorded data. Low pass filters helped us reduce the high-frequency noise induced by taking the derivative of the signals.

We experimented with low-pass filters of the 1st, 2nd, and 5th order. In Fig. 3.1, The red, yellow, purple, and blue lines represent the first-order filter, second-order filter, fifth-order filter, and original signal, respectively.

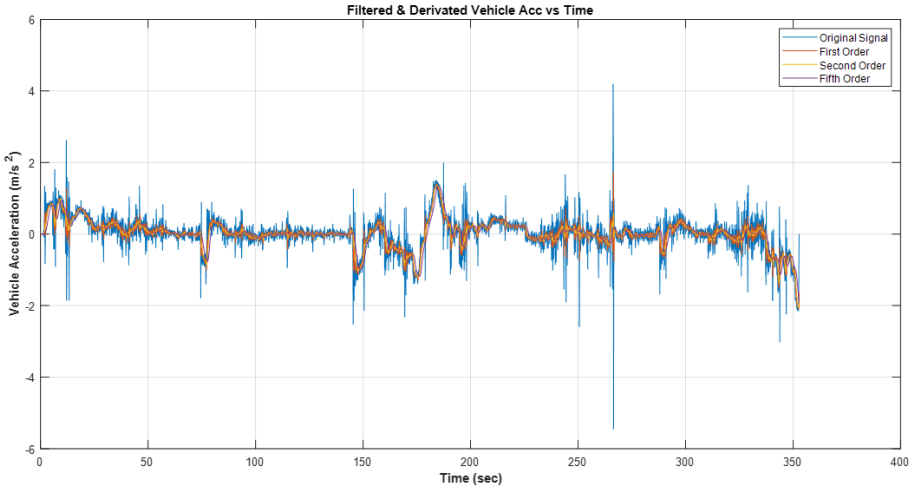

FIGURE 3.1: Comparison of The Different Order Filter on Vehicle Speed

Between the 1st and 2nd-order filters, there are minimal delays, the 2nd-order filter effectively reduces spikes without introducing significant delay. The 5th-order filter, while providing a smoother signal and further reducing spikes, introduces a noticeable delay interval.

Ideally, we aim to prevent spikes, particularly those arising from sudden noise, while still capturing meaningful signal changes. As observed, the 5th-order filter sacrifices responsiveness to change. Therefore, we selected the 2nd-order filter as it offers a balance between spike reduction and delay.

Acceleration is calculated from the speed data obtained from the EVCU by applying a second-order filter and a first-order derivative. We have selected a cutoff frequency of 4 Hz because our data is sampled at 100 ms (0.1 s) intervals, i.e. at 10 Hz which sets the Nyquist frequency to 5 Hz. We chose a 4 Hz cutoff to retain frequencies below 5 Hz and filter out those above.

Additionally, acceleration data from the Brake ECU was passed through the predefined second-order low-pass filter to obtain smoother data, as shown in Fig. 3.2. An added benefit of this filter is its suitability for real-time applications due to its causal nature.

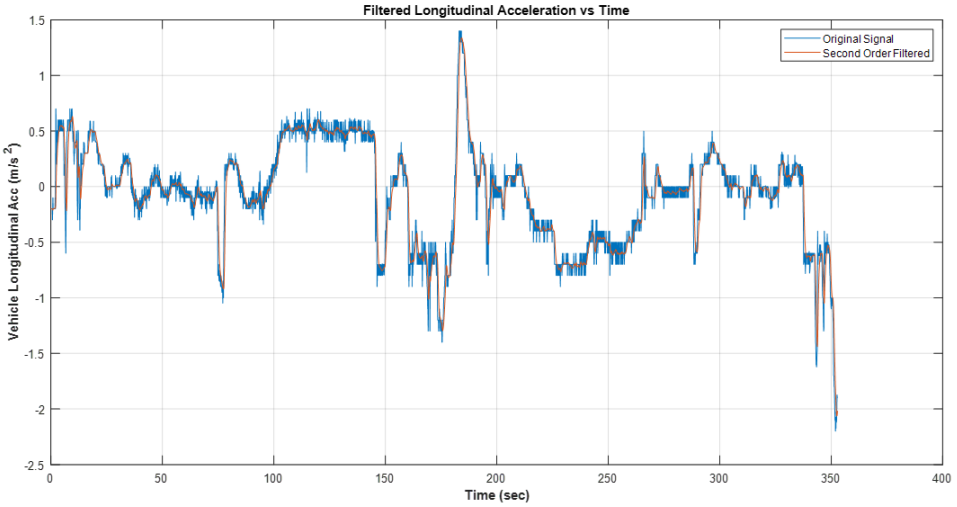

FIGURE 3.2: Filtered Longitudinal Acceleration

3.1.2 Obtaining the Longitudinal Speed

In our test vehicle, multiple sources of vehicle speed data are available on the CAN BUS. One of the method utilized for determining vehicle speed is managed by the EVCU, which calculates the vehicle speed based on motor speed (RPM) and converts it using the Eqn. 3.1.

$$V = \frac{N_p \cdot pi \cdot r_w}{30 \cdot gearratio} \tag{3.1}$$

where r_w is tire radius, G is the gear ratio, and n_p is motor rpm [21].

3.1.3 Obtaining the Vehicle Acceleration

We obtain acceleration data from two different ECUs in the vehicle. One is from the Brake ECU, which provides longitudinal acceleration calculated from the lateral acceleration and yaw sensor. The other one is obtained by taking the time derivative of the longitudinal speed that is calculated using the motor RPM.

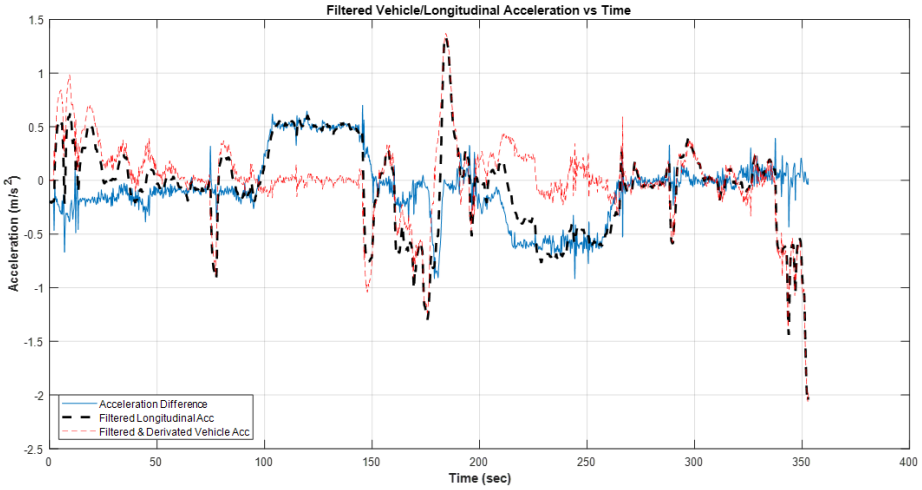

FIGURE 3.3: Acceleration Differences between Speed-Derived and Longitudinal Acceleration

The data obtained from the EVCU does not get affected by grade changes, while the data from Brake ECU, which utilizes in-house accelerometers, does. To analyze this effect, we compared the differences between the two data sets, as seen in the blue plot in Fig. 3.3. In the straight sections of the track, where we expect the data from both ECUs to align, we observed a deviation in the Brake ECU data compared to the EVCU. We primarily attribute this discrepancy to the road grade. Some other factors such as road conditions, braking, and cornering effects would also introduce a gap. Furthermore, the Brake ECU data-sheet does not list longitudinal acceleration as a directly measured parameter, suggesting that the Brake ECU relies on individual wheel sensors and assumptions in its calculations, which can introduce inaccuracies. For example, as shown by a red ellipse in Fig. 3.4, a discrepancy emerges as the vehicle makes a U-turn.

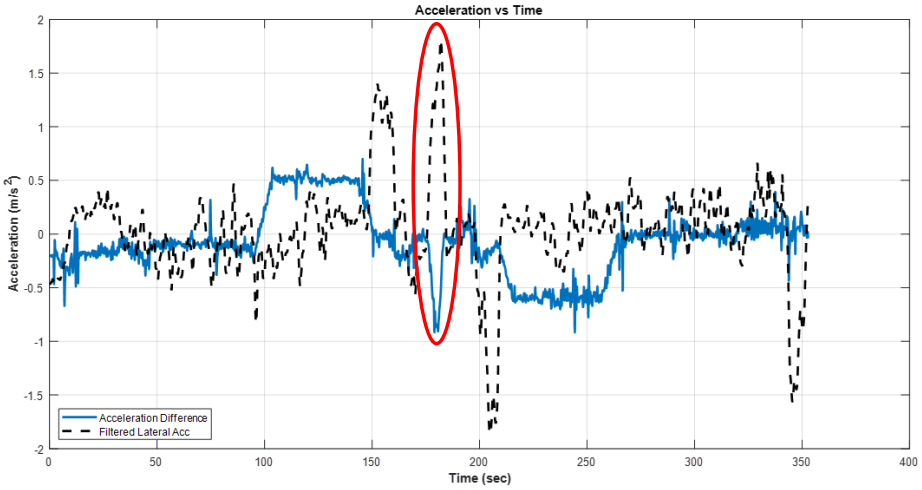

FIGURE 3.4: U-Turn Effect on the Accelerations

3.1.4 Road Grade

The road grade induces a difference between the accelerometer readings and numerically obtained longitudinal acceleration. Therefore, that difference could be used for obtaining the inclination angle of the road as follows [9]:

$$a_{sensor} = a_{vehicle} + g \cdot \sin\theta \tag{3.2}$$

$$\sin\theta = \frac{a_{sensor} - a_{vehicle}}{g} \tag{3.3}$$

where θ is the road grade, a_{sensor} is the acceleration signal from the on-board sensor, and $a_{vehicle}$ is the calculated longitudinal acceleration of the vehicle.

The resistive force due to road grade, then, becomes:

$$F_{grade} = m.(a_{sensor} - a_{vehicle}) \tag{3.4}$$

3.1.5 Obtaining the Traction Torque

In this study, two different torque data sources are utilized. The first was the instantaneous torque obtained directly from the motor, while the second was calculated using the Eqn. 3.5.

$$T_{motor} = F_{trac} \cdot gearratio \cdot r_w \tag{3.5}$$

where T_{motor} is the motor torque, and F_{trac} represents the sum of the resistive forces applied to the wheels in the longitudinal direction. F_{trac} calculation is presented in equation (2.6) [21].

3.1.6 Estimation of the Motor Torque using the Traction Force

A comparative analysis was conducted between two distinct sources of torque information: the first derived from calculated resistive forces based on vehicle parameters and driveline data, and the second obtained directly from the e-motor controller or inverter. The total resistive forces acting on the vehicle were calculated using Eqn. 2.1, and 3.5, excluding the grade effect, with adjustments made for vehicle-specific parameters. This analysis highlighted key discrepancies between the modeled resistive forces and the directly measured torque data.

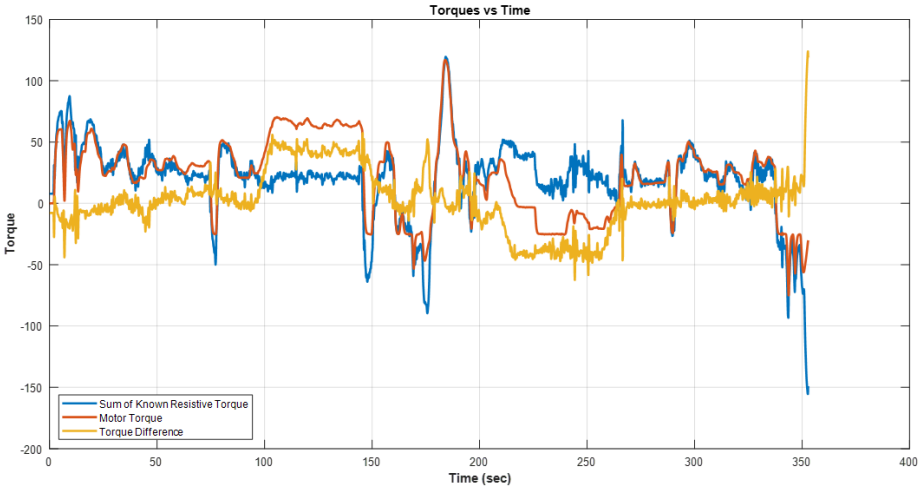

FIGURE 3.5: Torque Differences between Sum of Know Resistive Torque and Motor Torque

As illustrated in Fig. 3.5 , the differences, hereafter referred to as "residual torque," between the sum of resistive torques and motor torque exhibit significant variation in specific regions. These discrepancies are particularly evident on inclines and declines, during braking, and in sharp turns. In Fig. 2.17, these variations are highlighted at specific points corresponding to sharp turns (1, 2 and 4) and the uphill and downhill sections (3) of the route.

3.1.7 Correlation Between the Residual Torque and Residual Acceleration

During the analysis of the differences between the two acceleration data sets, it was hypothesized that these discrepancies might indicate the presence of grade effects. A similar trend was observed in the torque data, which led to the application of normalization techniques to explore the potential correlation between these variables.

In Fig. 3.6, the blue line represents the normalized residual torque, while the red line illustrates the normalized acceleration differences. The analysis reveals that decreases in residual torque correspond to decreases in acceleration differences.

Although certain anomalies, such as unexpected drops and rises, are present, the overall patterns of the two plots exhibit a strong alignment.

These findings suggest a relationship between the unexplained residual torque and acceleration differences, indicating a correlation with the resistance force associated to road grade. In Fig. 3.6, both variables exhibit similar responses during the 100-150 and 210-270 second intervals. These intervals correspond to segments of the test track in which the vehicle was ascending and descending slopes. The road grade is then calculated accordingly [9].

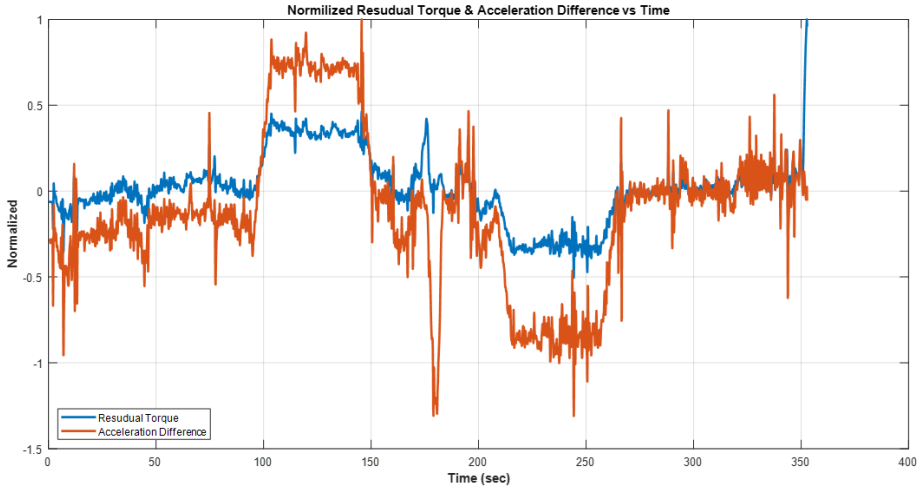

FIGURE 3.6: Normalized Residual Torque and Acceleration Differences

3.1.8 Motor Torque Estimation with the Effects of Road Grade Included

The resistive torque was recalculated by integrating the calculated grade effect. In Fig. 3.7 presents a comparative analysis, where the yellow line represents the torque calculation excluding the grade effect, while the red line incorporates it. Additionally, the blue line depicts the motor torque data obtained directly from the inverter.

A detailed comparison between the red and yellow lines demonstrates a substantial improvement in torque estimation accuracy when the grade effect introduced,

reflecting the influence of the vehicle's weight on resistive force. The red line shows a significantly closer alignment with the actual motor torque (blue line). Although minor discrepancies are observed during the first half of the route—potentially due to limitations in the vehicle modeling or not modeled factors—the convergence of the red and blue lines in the second half indicates a marked enhancement in torque estimation accuracy following the incorporation of the grade effect.

Online estimation methods are designed to improve the accuracy of torque calculations. Given that the primary objective of this study is to enhance mass estimation alongside torque estimation, therefore the precise calculation of the grade effect is essential to achieving reliable results.

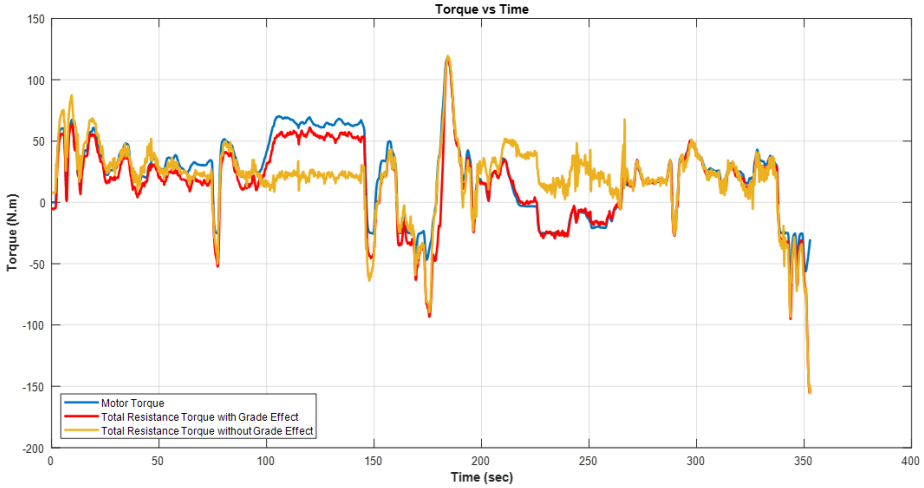

FIGURE 3.7: Road Grade Effect on Torque

3.2 Mass Estimation Algorithms

In this study, four different online estimation methods were analyzed to investigate the suitability of classical prediction-error-based online parameter estimation algorithms in the actual operation of the vehicle of interest. These methods are briefly explained as follows:

Gradient-Descent Estimator for the Vehicle Mass: Using the longitudinal vehicle dynamics model, the torque load on the motor can be estimated as follows:

$$\hat{T}_{motor} = m.(a_{vehicle} + (a_{sensor} - a_{vehicle}).c_{torque}) + F_{drag}.c_{torque} + F_{roll}.c_{torque} \quad (3.6)$$

where c_{torque} is the coefficient that converts force into torque as shown in equation (3.4). Since the torque due to road grade and the inertial force both depend on the mass, the regressor of the vehicle mass is comprised of the associated factors.

The error in the torque estimation is:

$$\tilde{T}_{motor} = \tilde{m}((a_{vehicle} + (a_{sensor} - a_{vehicle})c_{torque})) \quad (3.7)$$

where $\tilde{m}$ denotes the error in the parameter. The error in the torque estimation is obtained by comparing the estimated torque to the measured torque obtained using the drivers of the motor.

The estimation law is, then [25]:

$$\dot{\hat{m}} = p_0((a_{vehicle} + (a_{sensor} - a_{vehicle})c_{torque}))\tilde{T}_{motor} \quad (3.8)$$

where p_0 is the gain of the estimator.

Recursive Least Squares (RLS) Method for Estimating the Vehicle Mass: Suppose P is the estimator gain matrix. The parameter update rule is derived via RLS as follows [25]: Let k be the parameter update gain:

$$k = \frac{P.(a_{vehicle} + (a_{sensor} - a_{vehicle})c_{torque}))}{1 + P(a_{vehicle} + (a_{sensor} - a_{vehicle})c_{torque}))^2} \quad (3.9)$$

$$\dot{\hat{m}} = k.\tilde{T}_{motor} \quad (3.10)$$

where

$$\dot{P} = -k.((a_{vehicle} + (a_{sensor} - a_{vehicle})c_{torque})).P \quad (3.11)$$

and $P_{(0)} = 1000$.

Recursive Least Squares (RLS) with Forgetting Factor for Estimating the Vehicle Mass: Suppose P is the estimator gain matrix. In this method, the RLS algorithm involves a forgetting factor. The resulting estimation model becomes as follows [25]:

$$\dot{\hat{m}} = k.\tilde{T}_{motor} \tag{3.12}$$

where

$$\dot{P} = -k.((a_{vehicle} + (a_{sensor} - a_{vehicle})c_{torque})).P/\lambda \tag{3.13}$$

and λ is the forgetting factor that was set to 0.995.

Recursive Least Squares (RLS) with Multiple Forgetting Factors for Estimating both the Vehicle Mass and Road Grade: This time the road grade is also assumed as unknown and estimated along with the vehicle mass simultaneously. Since the road grade may change more rapidly, the forgetting factor associated with the road grade is lower ($\lambda_1 = 0.95$) than the vehicle mass ($\lambda_2 = 0.999$).

Chapter 4

Results

The study was organized around five distinct cases that are intended to evaluate the performance and accuracy of mass estimation algorithms under a variety of conditions, as outlined in Section 2.4.

This section presents an in-depth examination of the driving data collected across all five cases, accompanied by the estimated torque and vehicle weight values derived during the tests with their true values. These results are analyzed on a per-algorithm basis, utilizing the data retrieved from the vehicle's communication network throughout the driving sessions.

The mass estimation algorithms were applied under carefully defined conditions to ensure consistency and repeatability. These are: Gradient Descent, RLS, RLS with a Single Forgetting Factor, and RLS with Multiple Forgetting Factors. The use of these 4 algorithms allowed for a comparative analysis of their performance across various vehicle mass, road conditions, and driving style while the selection criteria of intervals for algorithm execution remained same across all cases and tests to ensure fairness in the evaluation.

Data input into the algorithms commenced as green zones in this section, when the vehicle's speed exceeded 40 km/h, and continued until either the brake pedal was applied or the speed dropped below 40 km/h showed as a red zone. This segmentation of the driving data was critical to standardizing the conditions under which

the algorithms were tested, and specifically for the comparison. The segmented data, represented as green zones in all mass estimation plots for the tests, were subsequently analyzed using the Absolute Mean Error (AME). A detailed table summarizing the results is provided in Section 5.

Although the same path was utilized in certain instances, there were substantial variations in the recorded data and driving characteristics as a result of differences in external and dynamic factors. For example, Case 1 and Case 2 were conducted on the same route but exhibited differences in driving style, external conditions and switching the start and end points of the case, which impacted the results. In contrast, Case 3 was performed on Track 2, providing a fresh perspective on the influence of route characteristics on algorithms mass and grade estimation performance. Additionally, Case 4 and Case 5 were derived as part of Track 2, which enhanced the diversity of the data set and allowed a more detailed examination of the algorithm's adaptability to diverse scenarios.

The Cases present the data with estimated torque and mass graphs for the tests. The mass estimations were evaluated and classified based on the AME metric for the comparison of scenarios/cases and algorithms.

4.1 Case 1

4.1.1 Test 1 - Vehicle at 3700 kg

The data from the first experiment of our cases are presented in Fig. 4.1. The first plot illustrates vehicle speed, the second plot displays steering angle sensor data, and the third plot shows brake information.

As observed, no braking occurs until the U-turn. Between 74 and 78 s, a sudden drop in the speed graph indicates a slight release of the acceleration pedal, triggered by regenerative brake. Approaching the U-turn, a positive change in

steering angle is observed, accompanied by a reduction in vehicle speed. This behavior suggests the vehicle entering the curve in Fig. 2.17 at 2.

A similar pattern is observed after the U-turn, where the steering angle shifts again, and the vehicle adjusts the speed naturally. The test was completed without applying the brakes again, all the way to the end of the track.

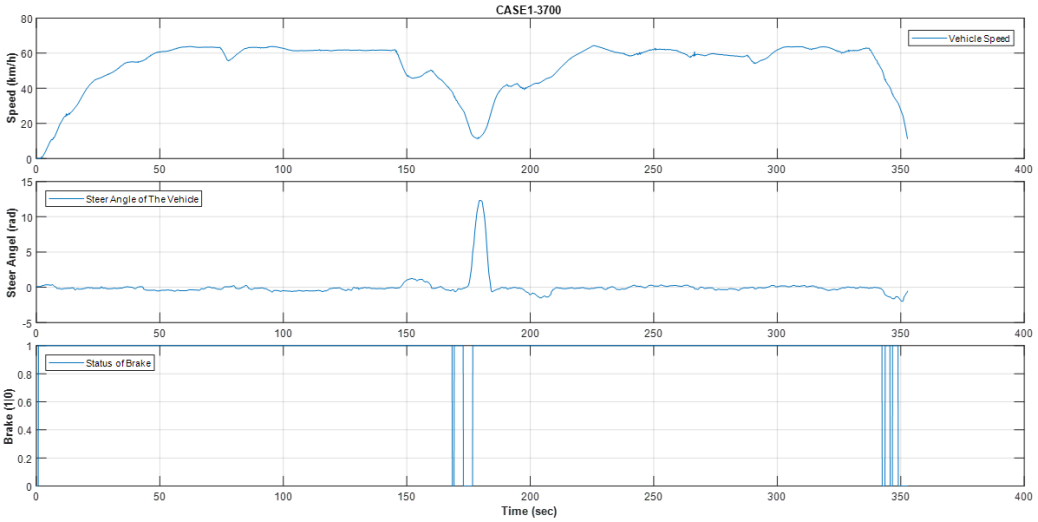

FIGURE 4.1: Speed, Steering Angle and Brake Profile of Test 1

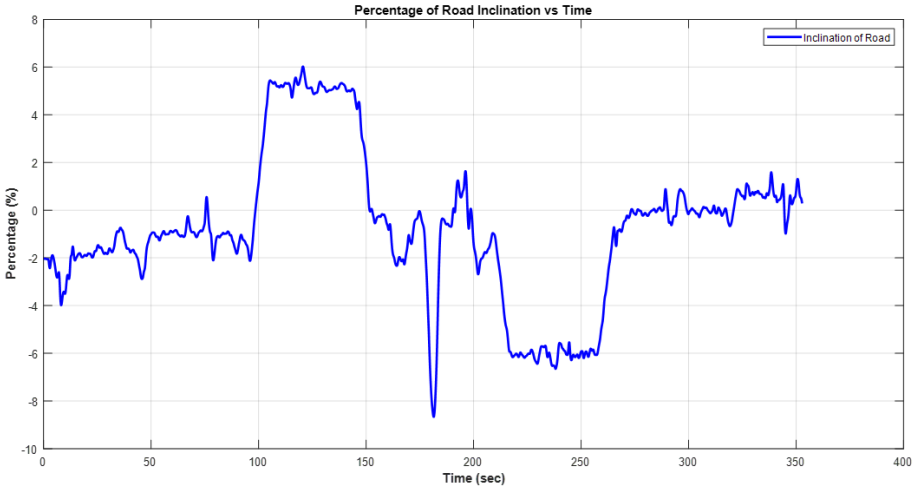

FIGURE 4.2: Track 1 Calculated Road Elevation Profile

In Fig. 4.2, the road grade was calculated using the Eqn. 3.3 in Section 3.1.4 and is illustrated accordingly. The uphill climb observed between 100-150 seconds

and the downhill descent along the same road between 220-270 seconds are clearly depicted in the figure.

4.1.1.1 Gradient Descent

In Fig. 4.3, the blue line represents the torque estimate updated online by dynamically adjusting the estimated mass. The yellow line indicates the torque estimation if the correct mass had been known, serving as a reference for the performance of the ideal model in this test. The purple line shows the scenario where the initial mass (set to 2000 kg) was used without updating; this demonstrates the impact of proceeding with an incorrect mass estimation on torque calculations. Finally, the red line represents the actual torque data obtained from the vehicle's ECU, reflecting the torque calculated by the motor.

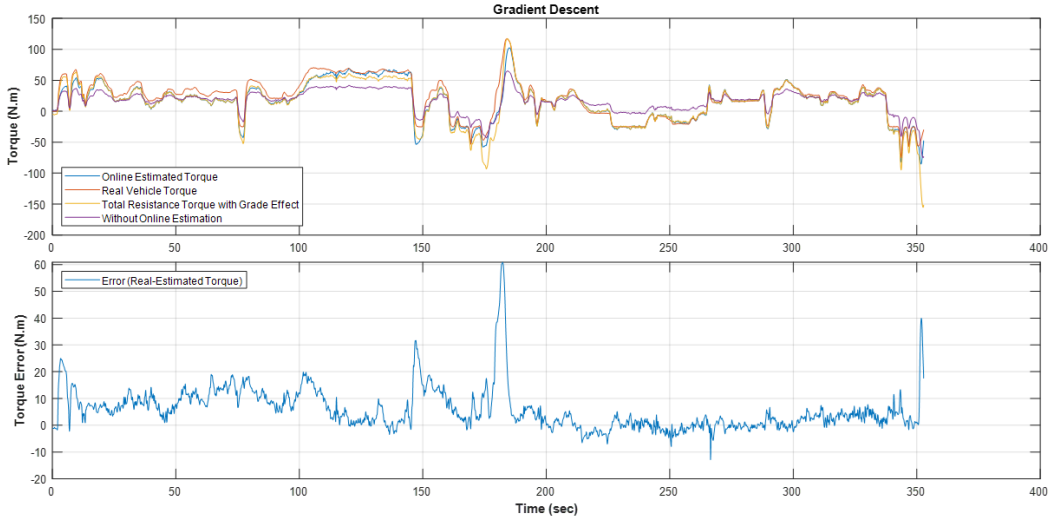

FIGURE 4.3: Torque Estimation Based on Gradient Descent Algorithm & Torque Error, Test 1

As seen in this Fig. 4.4 , the estimated mass calculated using the Gradient Descent algorithm is displayed. The red-shaded region between 0 and 20 s highlights the vehicle's acceleration phase, where vehicle reaches a speed of 40 km/h. Following this, the unshaded region represents a segment where the driver does not apply the brakes and the vehicle maintains a speed above 40 km/h. This segment is identified as suitable for AME calculations.

The number and duration of suitable segments vary across cases, influenced by factors such as road conditions, vehicle speed (represented by the data length in seconds), traffic density, and the presence of traffic lights. In Case 1, the mass estimation plots are divided into five distinct segments: three red-shaded regions, one unshaded region, and one green-shaded segment used for error calculations. Due to certain limitations, as discussed in Section 5, only the green-shaded region in the second half of the test (divided into pre- and post-U-turn phases) was selected for AME calculations.

The second red-shaded region in the middle of the figure corresponds to the U-turn segment (referred in Fig. 2.17 for the red path illustrating the U-turn as Section 1). Following the U-turn, the vehicle resumes cruising until the driver either reduces the speed below 40 km/h or applies the brakes. The final, red-shaded region marks the deceleration phase, where the driver applies the brakes to bring the vehicle to a complete stop.

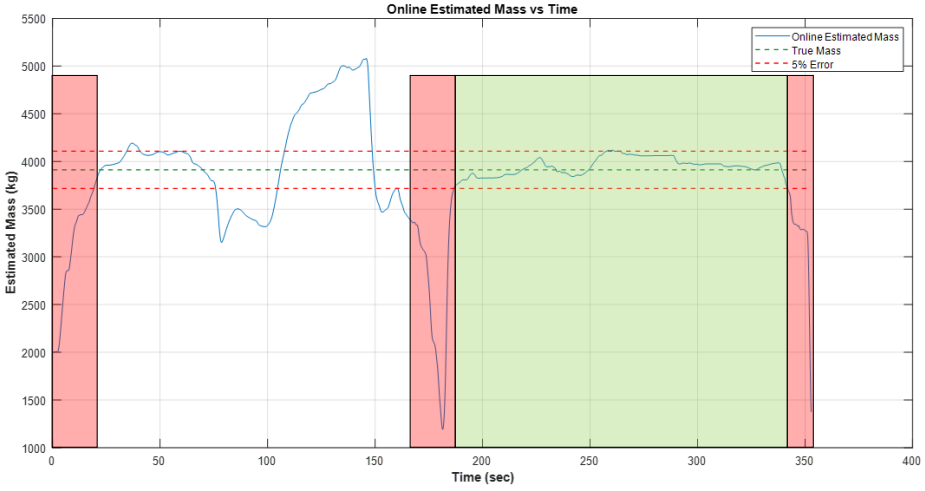

FIGURE 4.4: Mass Estimation Based on Gradient Descent Algorithm, Test 1

In Fig. 4.4, with a vehicle weight of 3700 kg, it is observed that the estimated mass remains within the 5% reference error margins in the green-shaded region, despite appearing somewhat fluctuating at times.

4.1.1.2 Recursive Least Squares

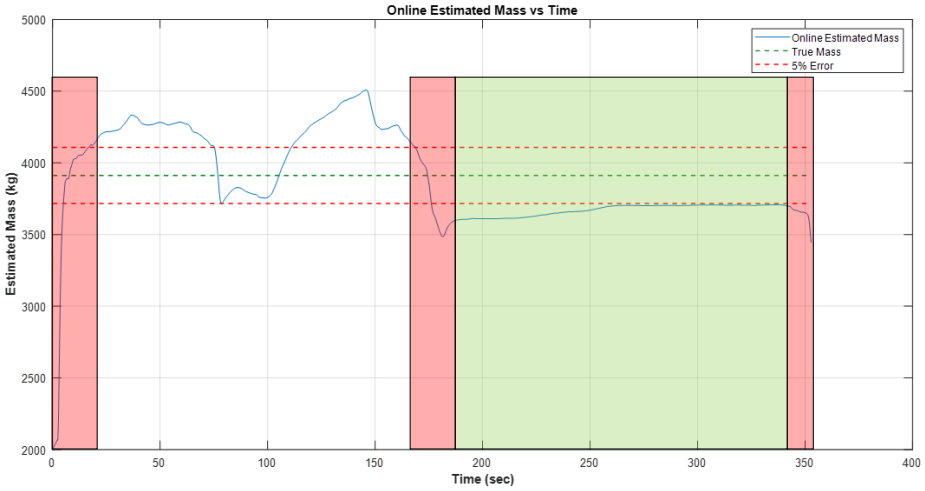

FIGURE 4.5: Mass Estimation Based on RLS Algorithm, Test 1

In the second half of the mass estimation using the RLS algorithm, a stable estimation is observed, as shown in Fig. 4.5, there is also less fluctuation in the torque error in this segment. However, the estimated vehicle mass falls outside the 5% error margin.

4.1.1.3 Recursive Least Squares with a Single Forgetting Factor

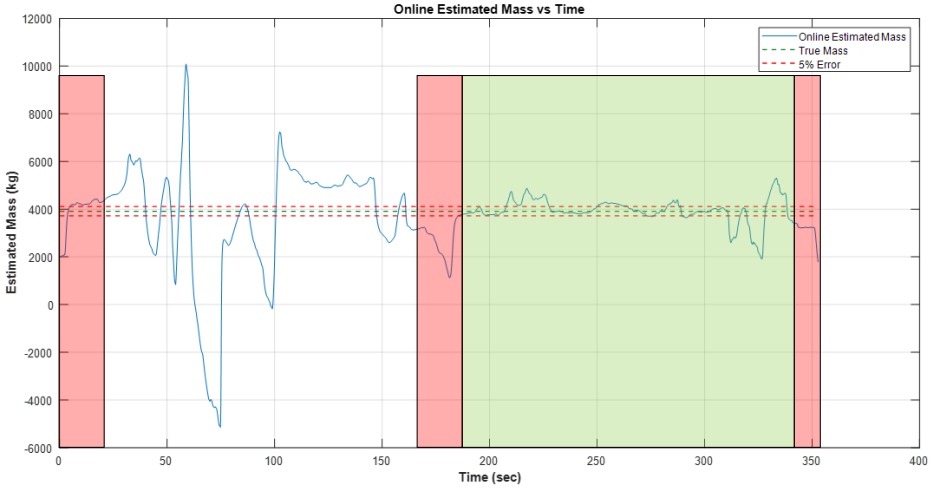

FIGURE 4.6: Mass Estimation Based on RLS with a Single Forgetting Factor Algorithm, Test 1

In the first segment of the mass estimation using the RLS algorithm with a forgetting factor, the estimated mass appears to have shifted into an unrealistic negative and positive range, as shown in Fig. 4.6. However, in the second segment, the estimation stays closer to the 5% range.

4.1.1.4 Recursive Least Squares with a Multiple Forgetting Factor

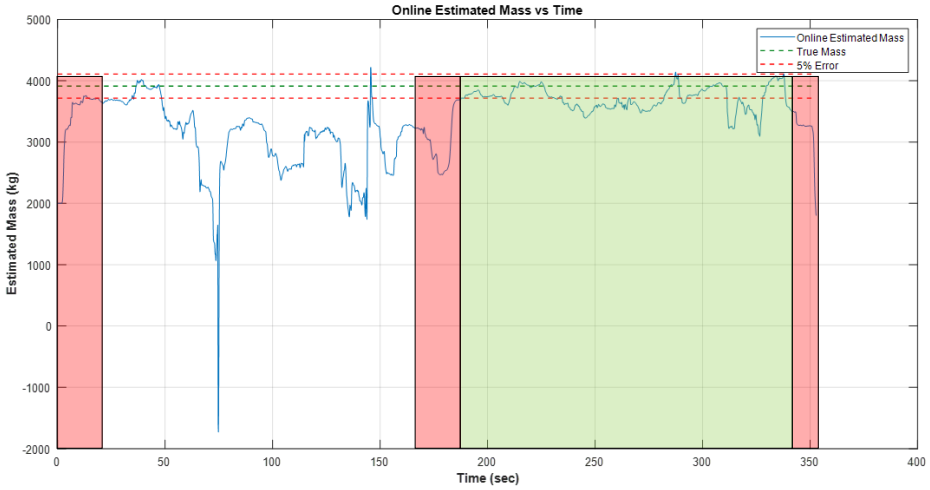

FIGURE 4.7: Mass Estimation Based on RLS with a Multiple Forgetting Factor Algorithm, Test 1

Similar to a single forgetting factor of RLS, the mass estimation in this scenario also shows unrealistic values in the first half in Fig. 4.7. However, unlike the previous estimations, it remains mostly below the upper bound of the 5% error margin. In the second half, the data show significant fluctuations, ranging between 5% and 10% errors.

4.1.2 Test 2 - Vehicle at 4200 kg

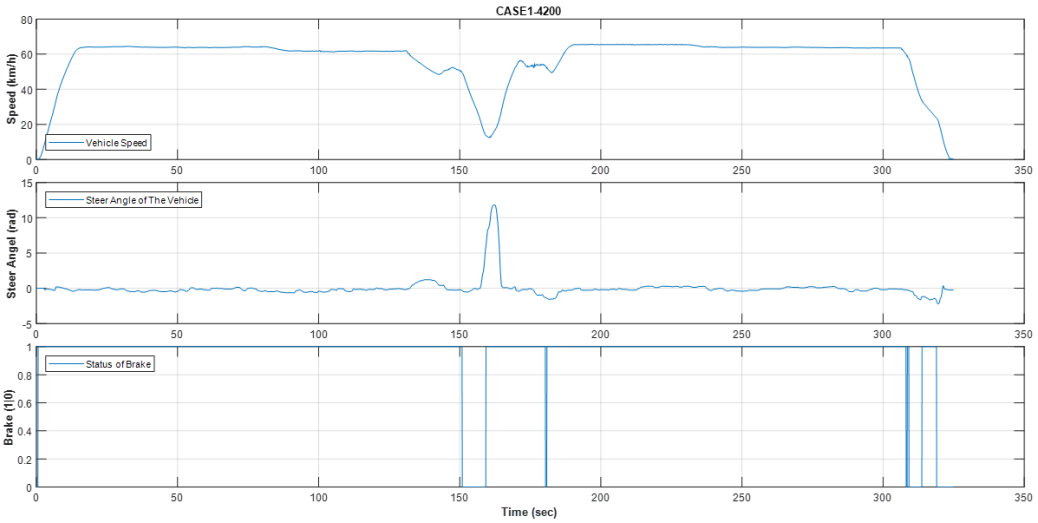

FIGURE 4.8: Speed, Steering Angle and Brake Profile of Test 2

With an additional 500 kg loaded on the curb weight of the vehicle, the driving data for Case 1, Test 2 is illustrated in Fig. 4.8. At points where the vehicle speed remains stable, the vehicle reaches its maximum allowable limit of 70 km/h as specified in the vehicle manual. However, due to regulatory constraints, the actual maximum speed is lower than seen on the cluster. Consequently, the plot has a consistent and flat regions, in contrast to the typical driving conditions.

4.1.2.1 Gradient Descent

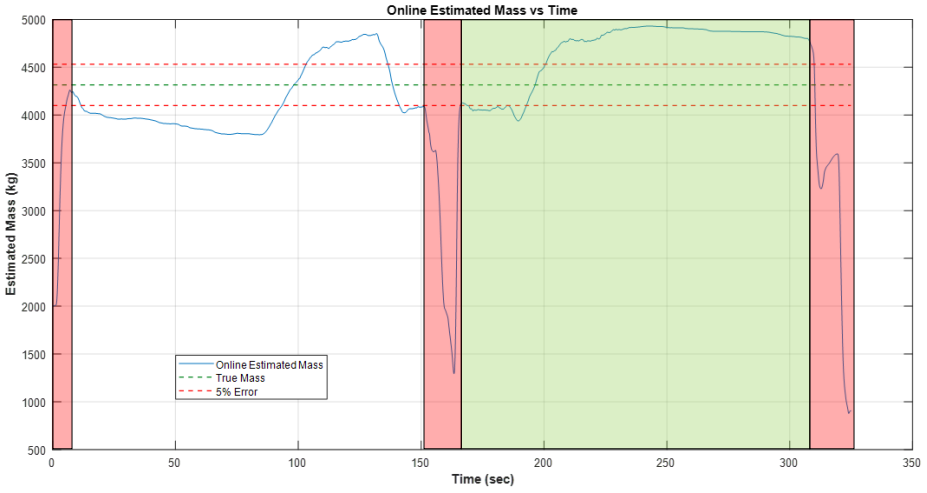

FIGURE 4.9: Mass Estimation Based on Gradient Descent Algorithm, Test 2

At the beginning of both the first and second segments in Fig. 4.9, the estimation hovers around the 5% error margin. However, it suddenly spikes, reaching up to 14% error, and in the second segment, it stabilizes at this level, continuing consistently until the end of the green segment. At the starting point of the test, corresponding to the first red segment, we observed that the limited range (narrow window) resulted from the vehicle quickly surpassing the 40 km/h threshold with fully pressing the accelerator pedal.

4.1.2.2 Recursive Least Squares

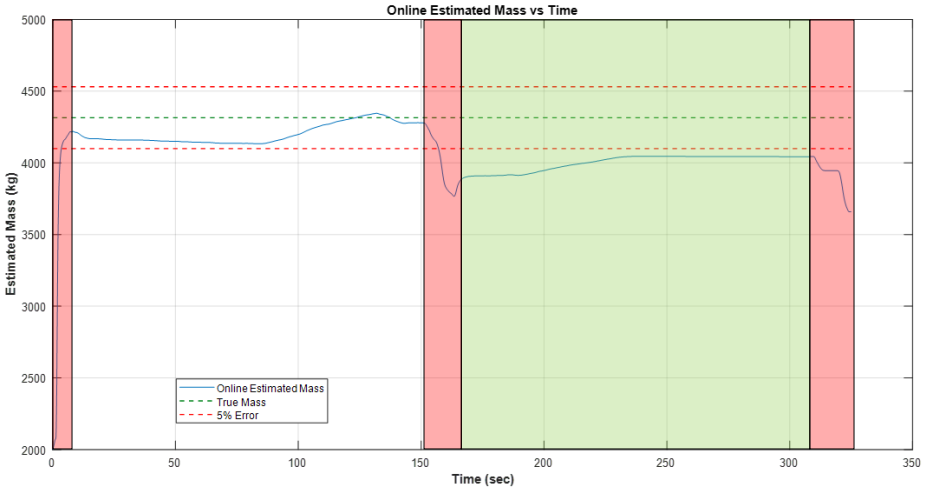

FIGURE 4.10: Mass Estimation Based on RLS Algorithm, Test 2

Although the mass estimation in the first half remained within the 5% error margin, the second half, which produced worse results in the graph, was evaluated for AME to ensure a more accurate comparison of the case and the study shown in Fig. 4.10.

4.1.2.3 Recursive Least Squares with a Single Forgetting Factor

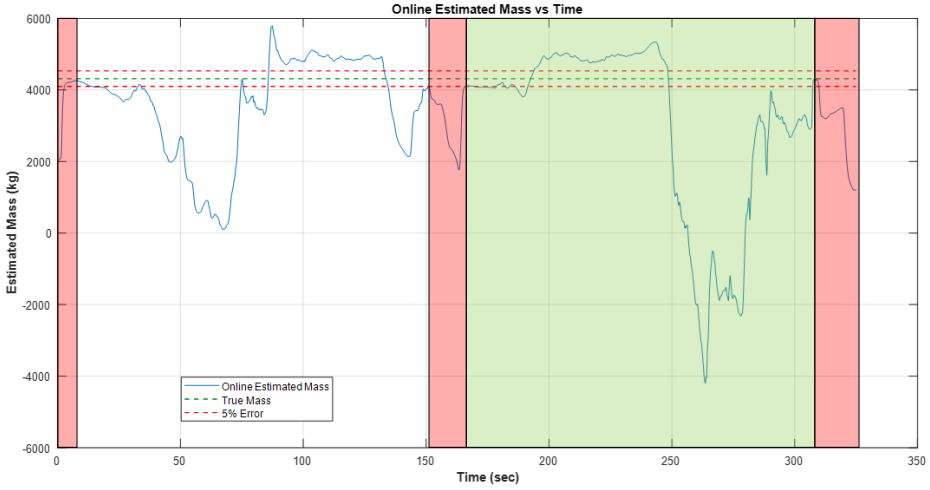

FIGURE 4.11: Mass Estimation Based on RLS with a Single Forgetting Factor Algorithm, Test 2

As seen in Fig. 4.6, in the 3700 kg test using the RLS algorithm with a single forgetting factor, the estimation plot dips into negative values in the first segment; similarly in the 4200 kg test, the mass estimation in the second half also reaches negative values in Fig. 4.11. Although it initially shows promising results after the U-turn, it begins to exhibit fluctuations after 180 seconds.

4.1.2.4 Recursive Least Squares with a Multiple Forgetting Factor

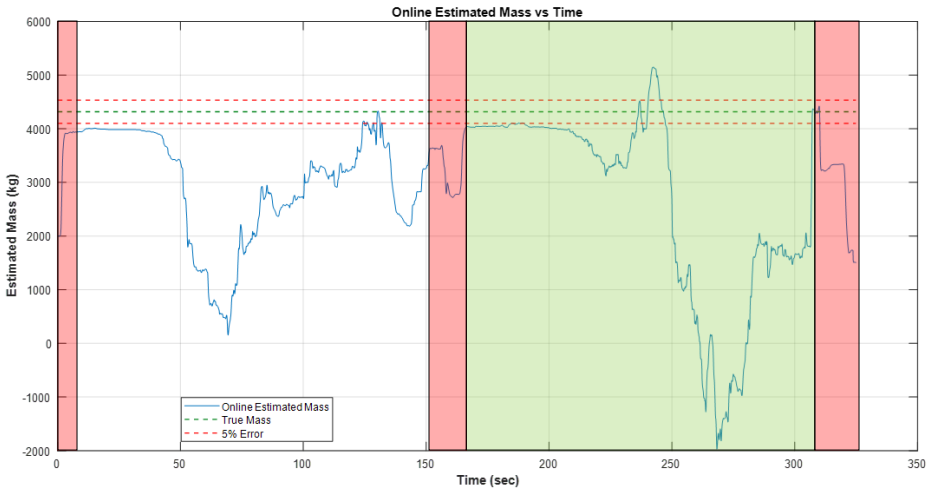

FIGURE 4.12: Mass Estimation Based on RLS with a Multiple Forgetting Factor Algorithm, Test 2

At the beginning of both the first and second half in Fig. 4.12, the estimations remain stable within the error margin 5%. However, they exhibit significant deviations as the test progresses. In particular, in the second half, negative estimation values are observed, resulting in around 40% AME.

4.1.3 Test 3 - Vehicle at 4600 kg

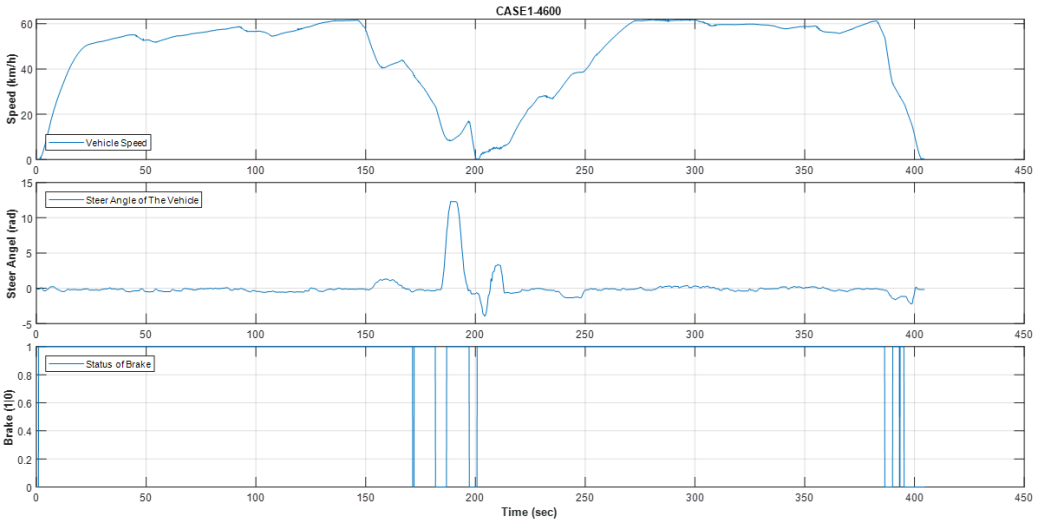

FIGURE 4.13: Speed, Steering Angle and Brake Profile of Test 3

Test 3, conducted with a total vehicle weight of 4810 kg, resulted in the longest track completion time among Case 1. The increased weight led to significant differences in both acceleration and deceleration dynamics compared to previous tests. Specifically, the U-turn deceleration and subsequent acceleration phase in Fig. 4.13 between 170 and 250 s, defined by the 40 km/h threshold, required more than twice the duration observed under similar conditions during previous tests.

4.1.3.1 Gradient Descent

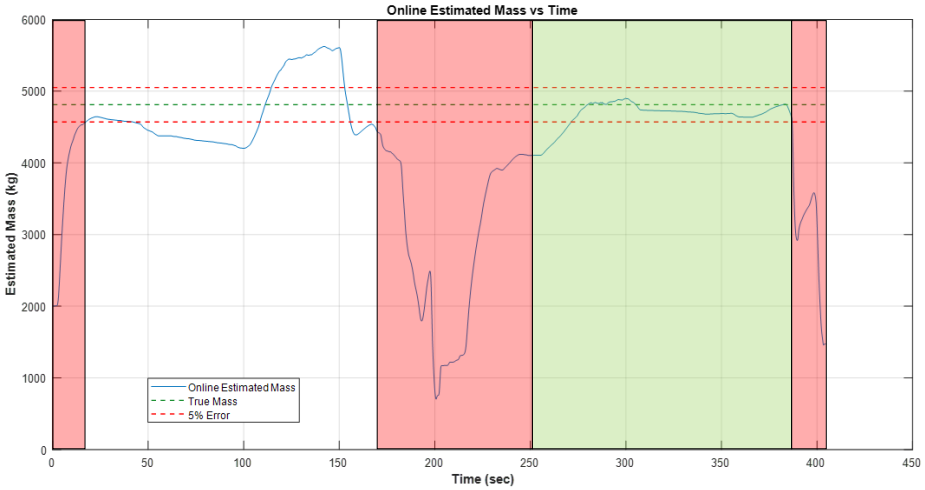

FIGURE 4.14: Mass Estimation Based on Gradient Descent Algorithm, Test 3

In the green-shaded region, the estimation begins with prediction of around 4100 kg vehicle mass and, after the 275th second, stabilizes within a 1- 3% error margin, closely aligning with the true mass. In this test, the red-shaded regions, where AME could not be performed, account for more than one-third of the total duration of the test in Fig. 4.14.

4.1.3.2 Recursive Least Squares

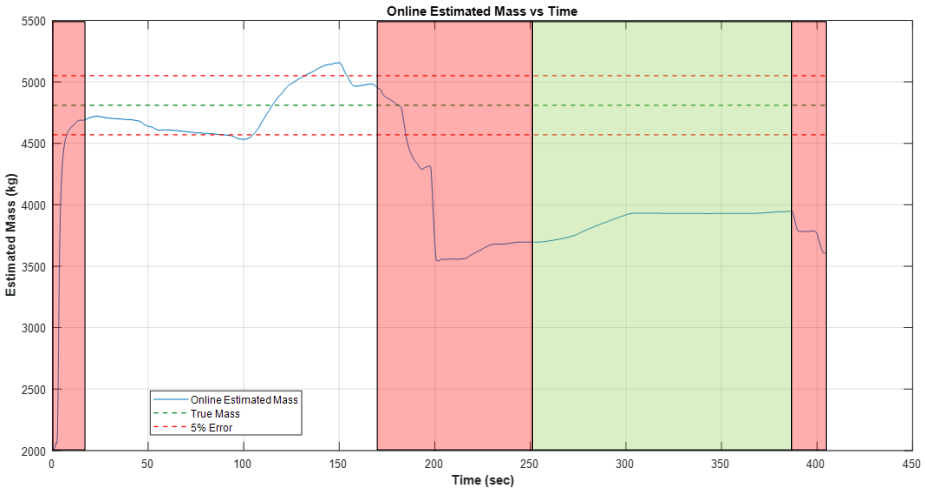

FIGURE 4.15: Mass Estimation Based on RLS Algorithm, Test 3

In the second half of Fig. 4.15, the estimation algorithm consistently predicts a vehicle weight of approximately 3900 kg. However, the RLS algorithm appears to struggle with recovery after the U-turn, at this value stabilized but with an unacceptable error margin.

4.1.3.3 Recursive Least Squares with a Single Forgetting Factor

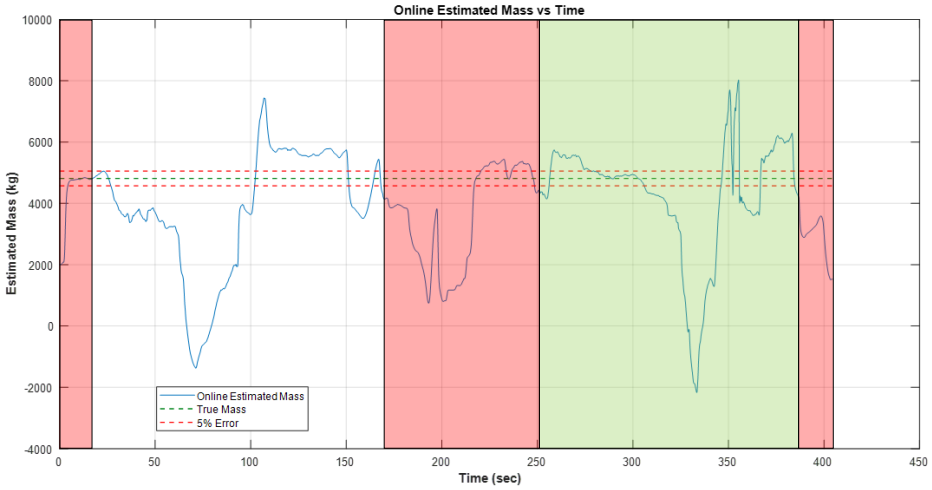

FIGURE 4.16: Mass Estimation Based on RLS with a Single Forgetting Factor Algorithm, Test 3

In this test, we observe the appearance of unrealistic and negative values in mass estimations in Fig. 4.16, similar to the patterns previously identified in the RLS algorithms with a forgetting factor.

4.1.3.4 Recursive Least Squares with a Multiple Forgetting Factor

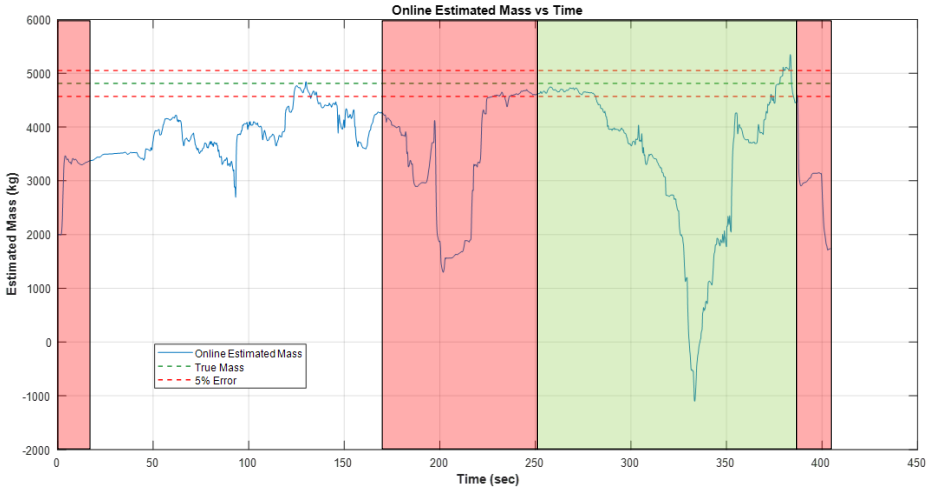

FIGURE 4.17: Mass Estimation Based on RLS with a Multiple Forgetting Factor Algorithm, Test 3

In the first segment, the estimation starts with a poor performance not observed in other tests, entering the 5% error margin range only briefly in a very small portion of the green-shaded region in Fig. 4.17. Besides this, continuous fluctuations are observed throughout the test.

4.1.4 Test 4 - Vehicle at 5000 kg

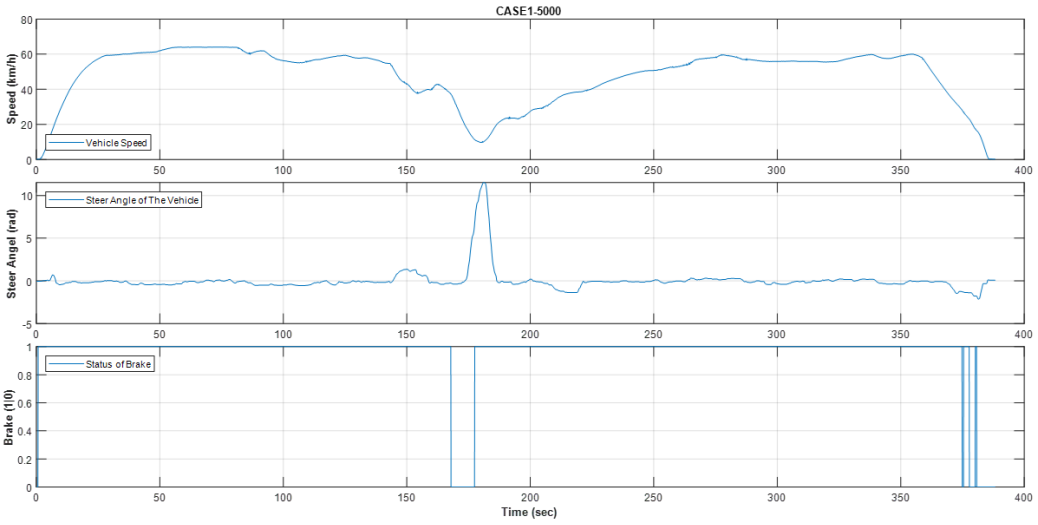

FIGURE 4.18: Speed, Steering Angle and Brake Profile of Test 4

This experiment, the final test of Case 1, was conducted with a total vehicle weight of 5810 kg. A significant increase in the time required to reach top speed can be observed by comparing in Figures 4.8 and 4.18. Notably, in the segment following the U-turn, it took approximately 1.3 minutes to reach a speed of 60 km/h. Although the first half of the route was more conducive to acceleration, allowing the vehicle to reach its top speed, the second half did not exceed 60 km/h. This limitation was primarily due to the driver's perception and caution, rather than the vehicle's capabilities, considering the increased weight and safety concerns.

4.1.4.1 Gradient Descent

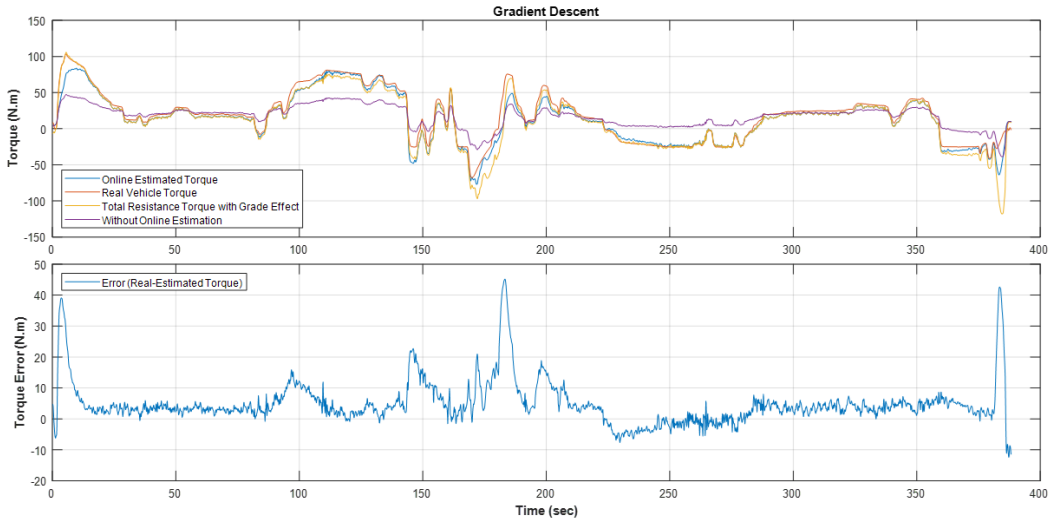

FIGURE 4.19: Torque Estimation Based on Gradient Descent Algorithm & Torque Error, Test 4

In Fig. 4.19, the effect of the increased mass is clearly observed. The purple line represents the calculation assuming a constant vehicle weight of 2000 kg, and it shows significant differences compared to the other lines in the plot, particularly during uphill and downhill segments which are before and after U-turn under increased total weight.

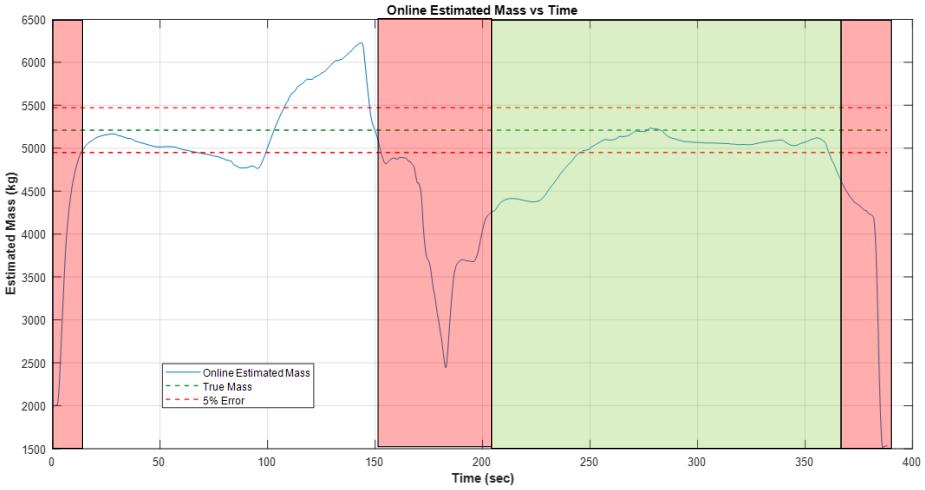

FIGURE 4.20: Mass Estimation Based on Gradient Descent Algorithm, Test 4

The estimation algorithm exhibited suboptimal performance at the beginning of the green-shaded region but stabilized within the 5% error margin after around 45 seconds. Compared to Test 3, conducted with a vehicle curb weight of 4600 kg, the red-shaded areas occupy a smaller portion of the test data. However, these regions are considerably more extensive than those observed in Test 1 and Test 2.

4.1.4.2 Recursive Least Squares

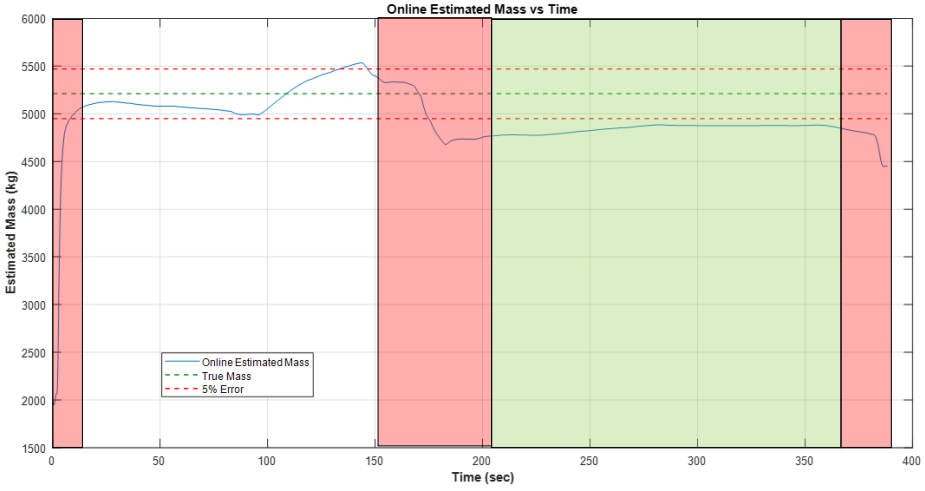

FIGURE 4.21: Mass Estimation Based on RLS Algorithm, Test 4

In the first half of the test, a significant portion of the data remain within the 5% error margin, indicating a relatively accurate estimation of mass during this phase, as seen in Fig. 4.21. In contrast, in the second half of the test, the estimation deviates slightly, stabilizing at a higher error level of approximately 7%. Despite this increased error margin, the plot exhibits remarkable consistency, suggesting that while the accuracy decreased, the algorithm managed to maintain stability in its predictions.

4.1.4.3 Recursive Least Squares with a Single Forgetting Factor

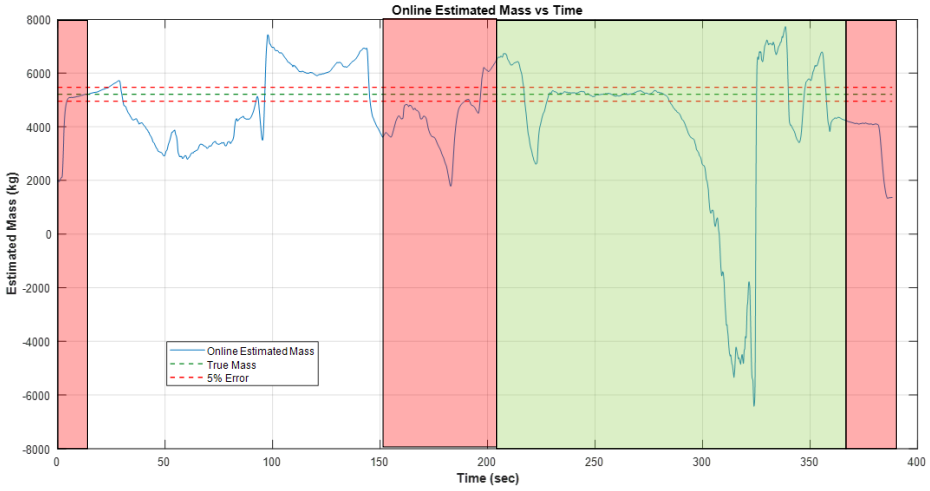

FIGURE 4.22: Mass Estimation Based on RLS with a Single Forgetting Factor Algorithm, Test 4

In Fig. 4.22, the plot begins in the green-shaded region and approaches nearly zero error within the first 20 seconds, maintaining this accuracy for approximately 50 seconds. However, following this stable period, the estimation suddenly diverges, resulting in an unrealistic negative mass value of -6000 kg. A similar phenomenon of negative estimation is observed in other Case 1 tests using the RLS algorithm with a forgetting factor.

4.1.4.4 Recursive Least Squares with a Multiple Forgetting Factor

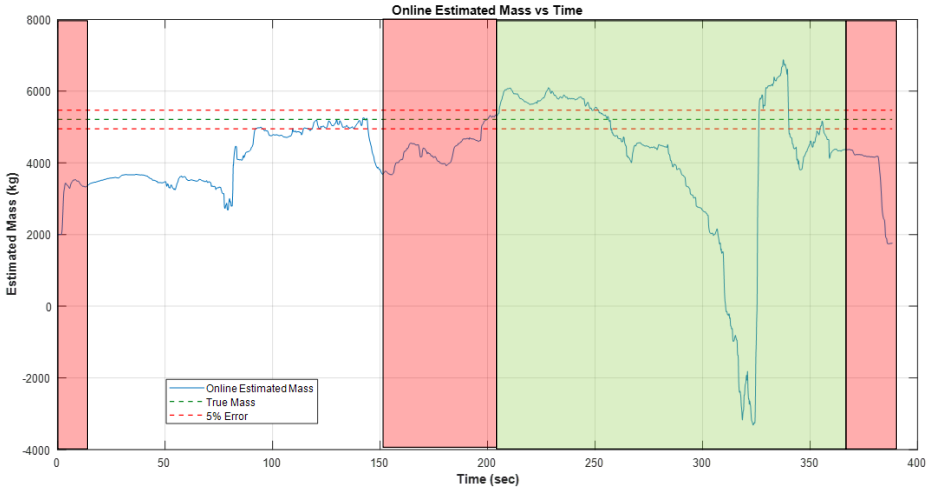

FIGURE 4.23: Mass Estimation Based on RLS with a Multiple Forgetting Factor Algorithm, Test 4

For all Case 1, a similar phenomenon is observed across RLS algorithms with forgetting factors. In single forgetting factor implementations, the estimation results range between +8000 kg and -6000 kg. In contrast, multi-forgetting factor implementations generally limited these unrealistic values to around -2000 kg for the lower sections of the multiple forgetting factor graphs.

In Fig. 4.23, the green-shaded region indicates estimation values around -3000 kg. Apart from a small section in the initial part with a relatively stable error of approximately 30%, no segment exhibits stability in any other parts that could be considered reliable in the error margin.

4.2 Case 2

4.2.1 Test 5 - Vehicle at 3700 kg

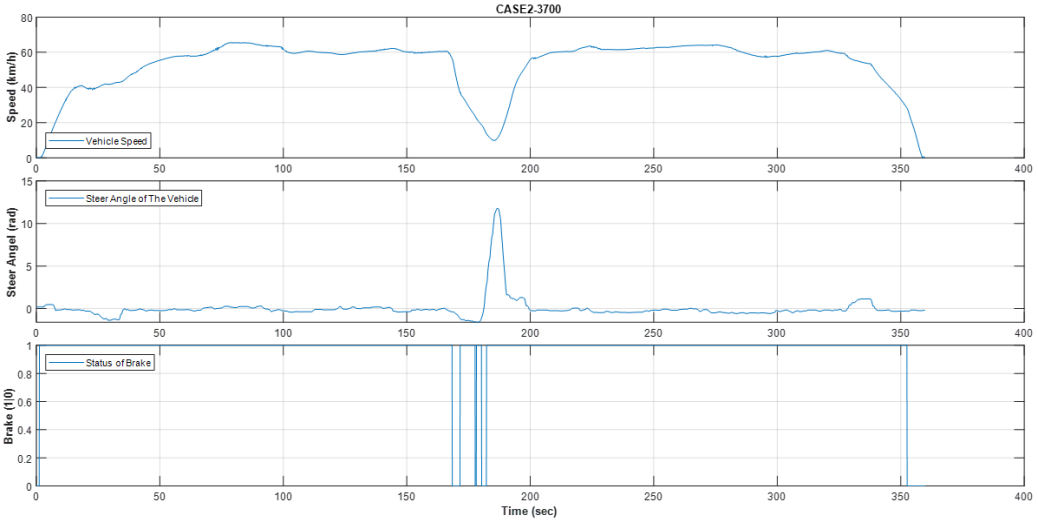

FIGURE 4.24: Speed, Steering Angle and Brake Profile of Test 5

In the Case 1, the beginning of the second segment (post-U-turn) shown in Fig. 4.1 demonstrates similar vehicle speed increments similar to the first segment of this case, observed within the 0-100-second range in Fig. 4.24. This similarity is further supported by the fact that both tests were conducted by the same driver and with identical vehicle weights, reinforcing this observation. In addition, it should be noted that the vehicle occasionally reaches its top speed during this test.

4.2.1.1 Gradient Descent

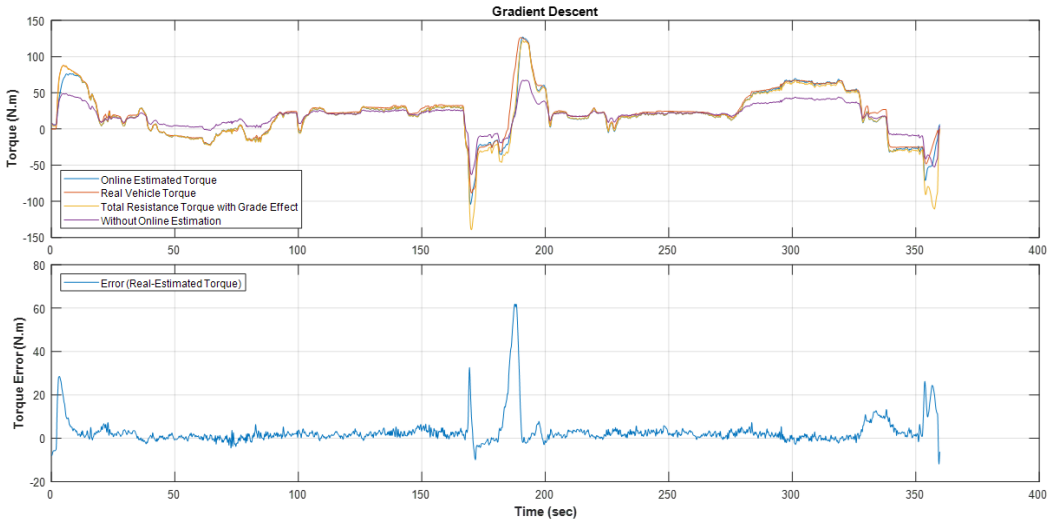

FIGURE 4.25: Torque Estimation Based on Gradient Descent Algorithm & Torque Error, Test 5

In Fig. 4.25, it can be seen that the estimated torque and the actual torque plots align almost perfectly, with only a few exceptional regions showing divergence. The reason for the occasional deviation of the purple line from the others is that the vehicle weight during the estimation process remains fixed at the predefined initial value of 2000 kg. In areas where the vehicle encounters ascents and descents, the real torque deviates from the estimated torque due to the grade effects, causing the purple line to diverge from the others.

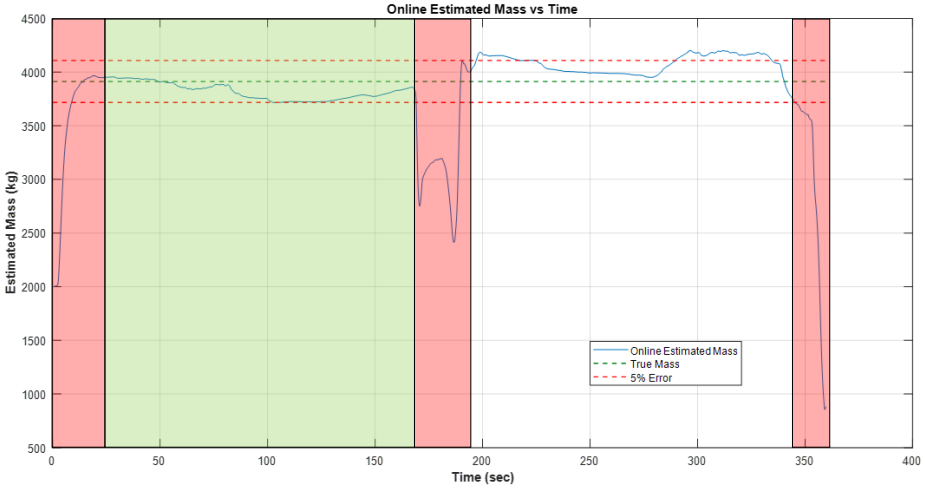

FIGURE 4.26: Mass Estimation Based on Gradient Descent Algorithm, Test 5

In Fig. 4.26, the mass estimation fluctuates within the error margin 5%, excluding the red-shaded regions. To more accurately compare Case 1 and Case 2 under varying scenario conditions, we have selected the downhill segment, corresponding to the first region in this case, for the AME calculations. Similarly to Case 1, where the downhill segment was shaded in green, this region has been selected to ensure consistency in the analysis.

4.2.1.2 Recursive Least Squares

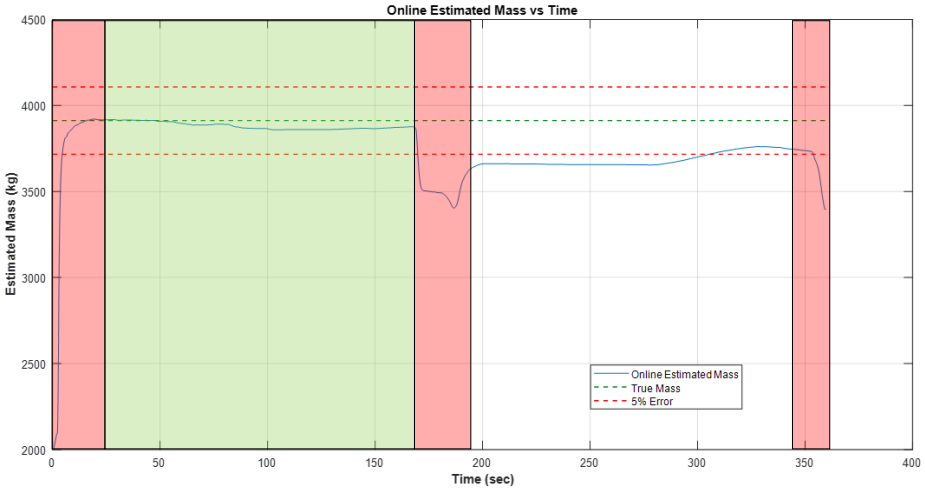

FIGURE 4.27: Mass Estimation Based on RLS Algorithm, Test 5

As seen in Fig. 4.27, the RLS estimation algorithm performs exceptionally well in the first segment, closely aligning with the true mass throughout this phase. However, a sudden drop in the estimation is observed after the brake is applied, corresponding to the red-shaded region. In the second half, while the mass estimation does not perform as well as in the first segment, it fluctuates within a 6-7% error margin. In particular, the excellent performance of the algorithm in the first segment is reflected in an AME score of 0.8%.

4.2.1.3 Recursive Least Squares with a Single Forgetting Factor

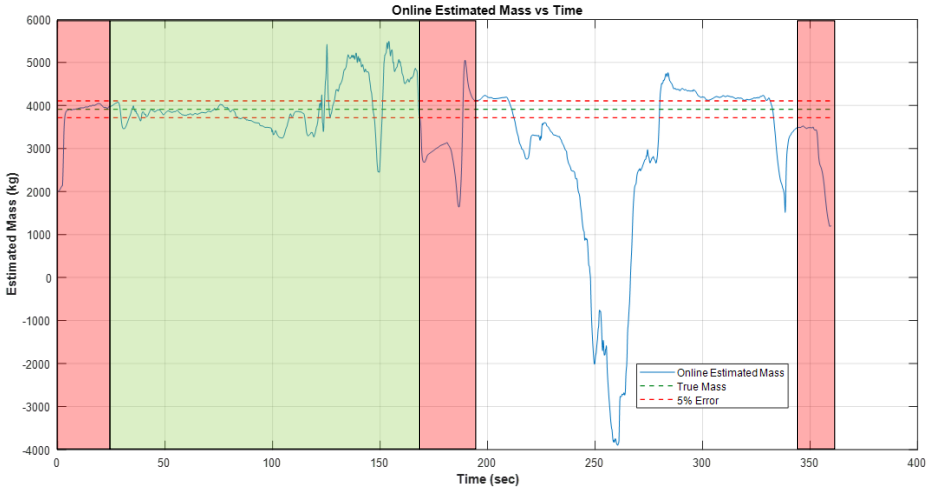

FIGURE 4.28: Mass Estimation Based on RLS with a Single Forgetting Factor Algorithm, Test 5

Although mass estimation begins accurately within the green-shaded region, a spike is observed later, as illustrated in Fig. 4.28. In the second segment, the mass estimations deviate significantly, reaching unrealistic values of approximately -4000 kg, similar to the behavior observed in Case 1 when using RLS algorithms with forgetting factors. Within the first red-shaded region, it is notable that the estimates align closely with the true value even before the vehicle reaches a speed of 40 km/h.

4.2.1.4 Recursive Least Squares with a Multiple Forgetting Factor

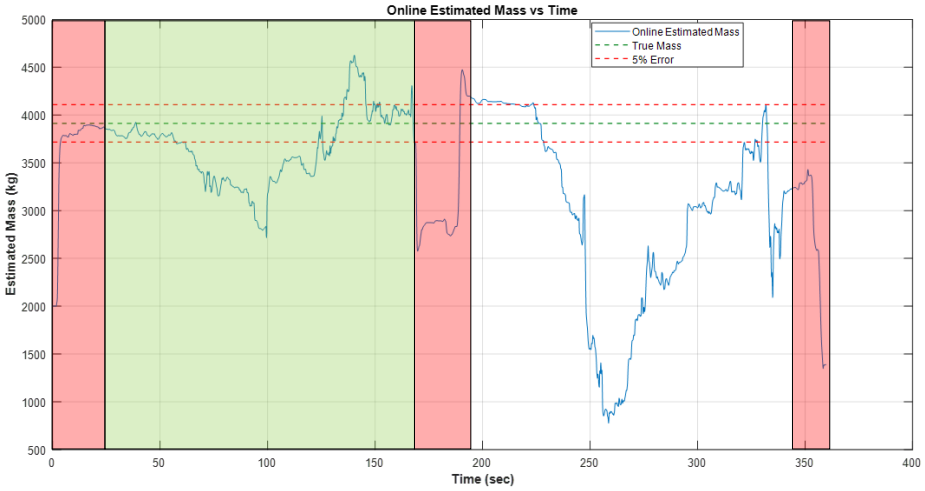

FIGURE 4.29: Mass Estimation Based on RLS with a Multiple Forgetting Factor Algorithm, Test 5

The RLS with a multiple forgetting factor estimate, as shown in Fig. 4.12, remains within the error margin 5% in the first region, although minor spikes are noticeable even in this segment. In general, the mass estimation based on multiple forgetting factors has not performed effectively.

4.3 Case 3

4.3.1 Test 6 - Vehicle at 3700 kg

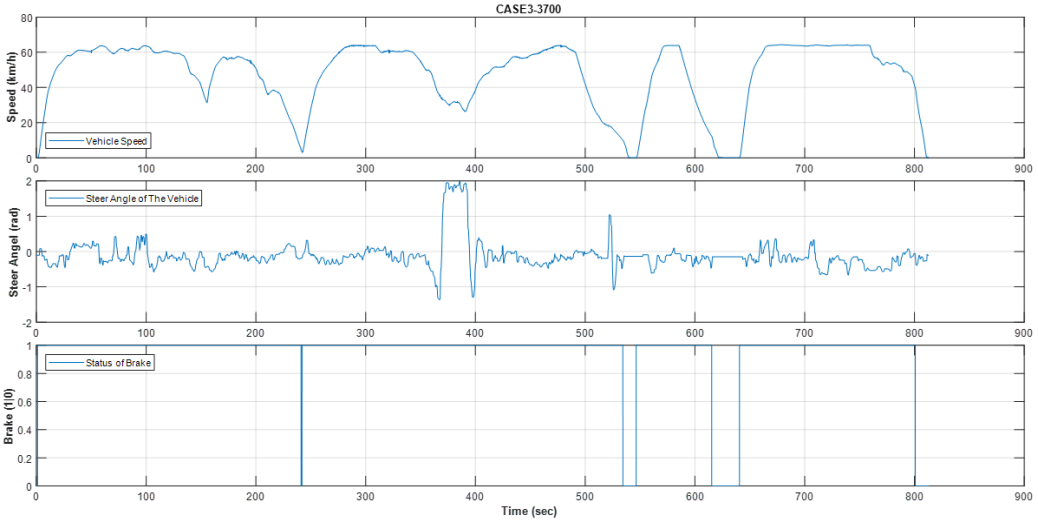

FIGURE 4.30: Speed, Steering Angle and Brake Profile of Test 6

As described in the beginning of Section 2.4, Case 3 was carried out under normal traffic conditions on a road with four traffic lights. An analysis of Fig. 4.30 reveals that the vehicle came to a complete stop at two traffic lights between 500 and 700 seconds. Additionally, during the 200-300 second interval, the vehicle decelerated to approximately 2-3 km/h before accelerating again.

Between 100 and 200 seconds, the vehicle approached a traffic light and decelerated using regenerative braking without applying the brakes. Upon the light turning green, the vehicle resumed acceleration and continued along the route. Between 350 and 400 seconds, a wide U-turn was executed, after which the vehicle proceeded along the opposite lane of the same road. The test was completed in approximately 800 seconds (13 minutes), concluding parallel to the starting point.

In general, the vehicle traversed the 10.3 km route with intermittent stops. As indicated by the steering angle plot and in Fig. 2.19, minor steering adjustments were made, reflecting a smooth and comfortable driving style throughout the test.

4.3.1.1 Gradient Descent

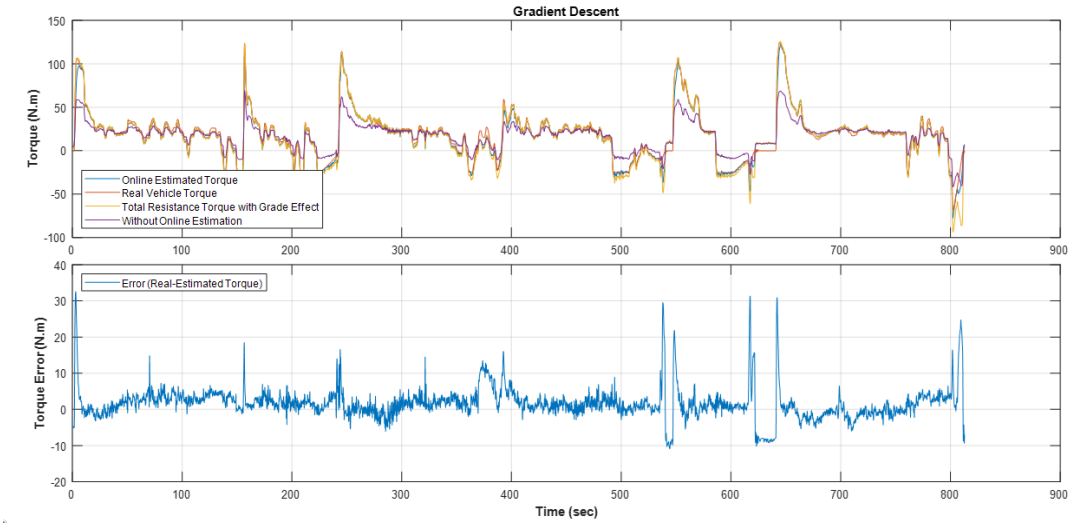

FIGURE 4.31: Torque Estimation Based on Gradient Descent Algorithm & Torque Error, Test 6

As depicted in Fig. 4.31, the frequent accelerations and decelerations observed during the test result in numerous spikes within the torque plots. In particular, during the intervals between 540 and 550 seconds and 620 and 640 seconds, a considerable divergence is observed between the estimated torque and the actual torque. Besides, these specific intervals indicate that the estimated torque consistently struggles to align with the actual torque during rapid variations, underscoring the difficulty of accurately capturing such dynamic changes.

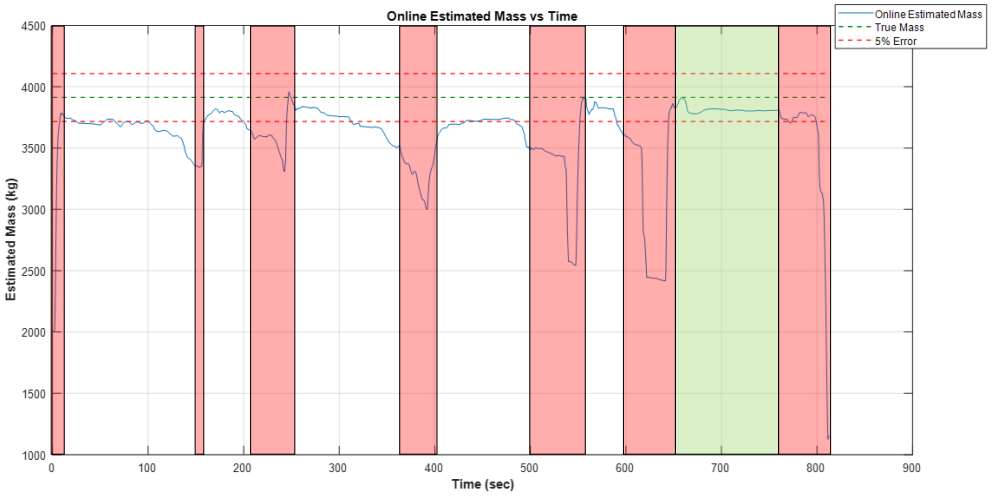

FIGURE 4.32: Mass Estimation Based on Gradient Descent Algorithm, Test 6

In this case, due to the frequent stop-and-go traffic conditions, 7 red-shaded sections appeared, resulted by below 40 km/h five times and braking was applied once, on the Gradient Descent plot, as shown in Fig. 4.32. The first red-shaded section corresponds to the initial period before the vehicle reached 40 km/h and was excluded from the evaluation. The green-shaded region was used as the reference range for AME calculations throughout all mass estimations in Case 3.

Overall, during normal driving conditions, the mass estimation remains around the 5% error margin. However, whenever the vehicle decelerates due to regenerative braking, the estimation experiences a negative impact, even before entering the red-shaded regions. This emphasizes the vulnerability of the estimation algorithm to deceleration events that are typically associated with regenerative braking.

4.3.1.2 Recursive Least Squares

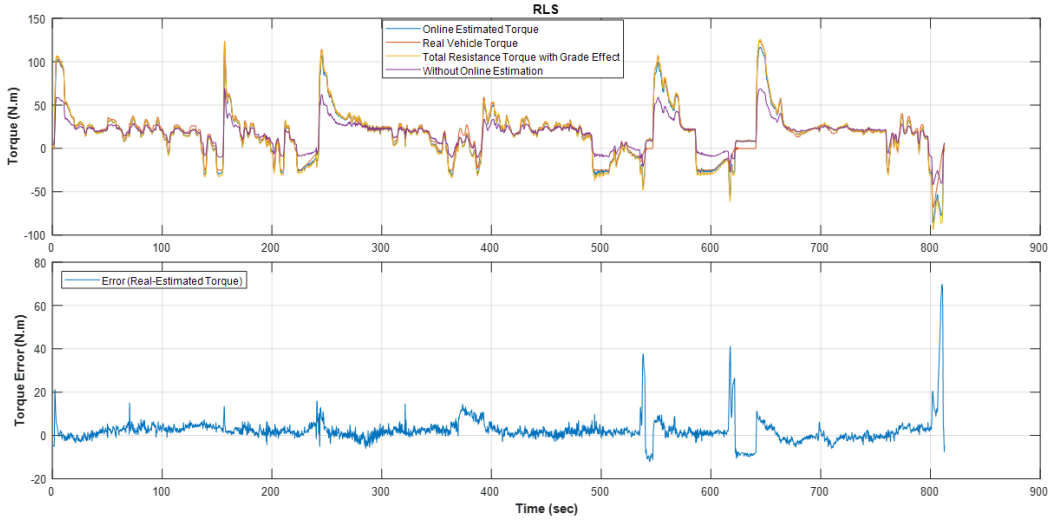

FIGURE 4.33: Torque Estimation Based on RLS Algorithm & Torque Error, Test 6

The divergence points between the real and estimated torques are clearly observable in the torque error in Fig. 4.33. Although the fluctuations are less pronounced compared to those seen in the Gradient Descent algorithm, the intervals of divergence identified in the previous analysis are also prominently reflected in the RLS algorithm's performance.

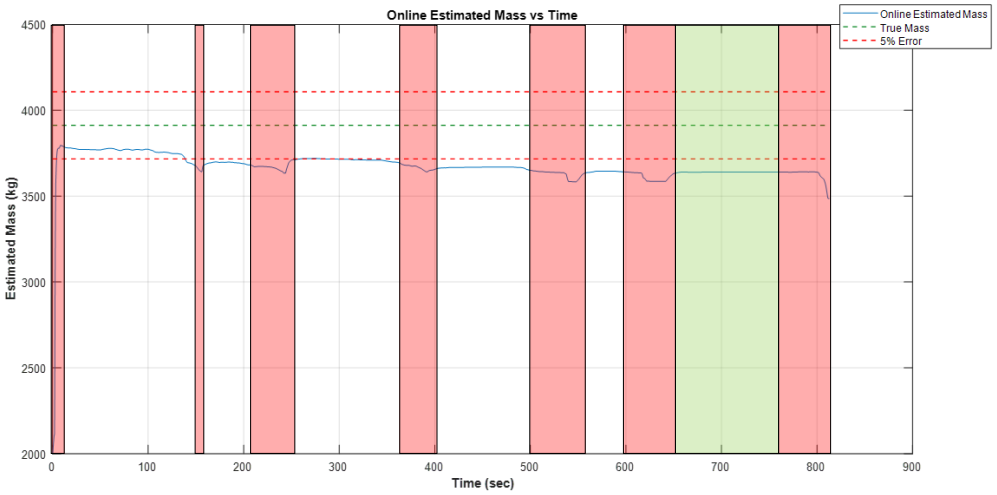

FIGURE 4.34: Mass Estimation Based on RLS Algorithm, Test 6

Mass estimations are observed to quickly reach a steady state in all non-red-shaded regions in Fig. 4.34. However, within the first 100 seconds, the estimation remains within the 5% error margin, while in the green-shaded region, it stabilizes at approximately 7% error.

4.3.1.3 Recursive Least Squares with a Single Forgetting Factor

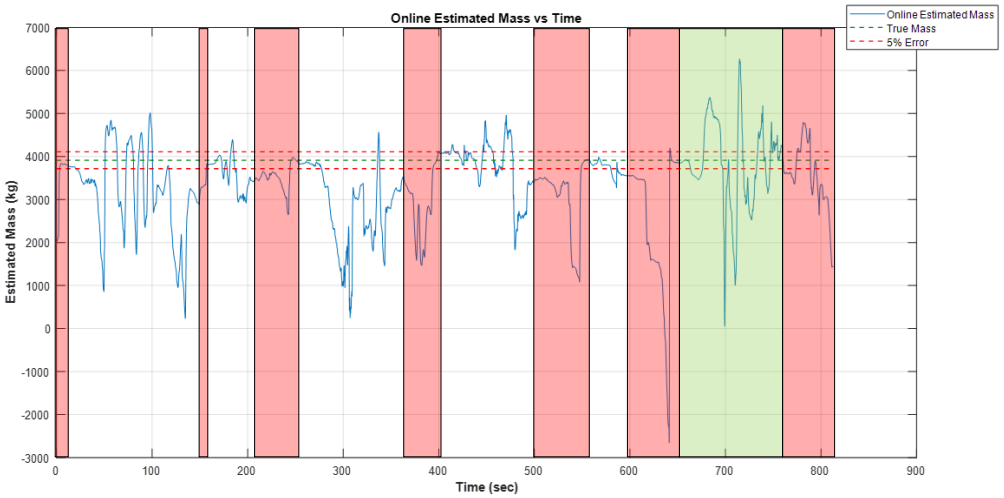

FIGURE 4.35: Mass Estimation Based on RLS with a Single Forgetting Factor Algorithm, Test 6

As observed in Case 1, the estimation profiles with forgetting factors exhibit similar behavior in the stop-and-go test, as shown in Fig. 4.6 and 4.35. Both the torque and mass estimations display highly fluctuating outputs without any steady-state region. Additionally, the estimated vehicle weight occasionally drops below 1000 kg, with one instance approaching the -3000 kg range.

4.3.1.4 Recursive Least Squares with a Multiple Forgetting Factor

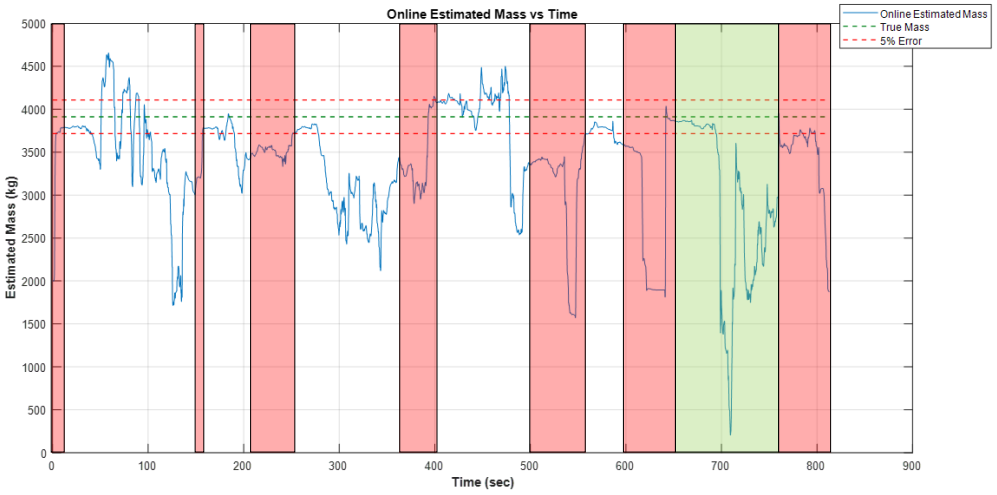

FIGURE 4.36: Mass Estimation Based on RLS with a Multiple Forgetting Factor Algorithm, Test 6

The same pattern observed in RLS with a single forgetting factor is also seen in Fig. 4.36 for the estimation of the mass of RLS multiple forgetting factors. Although the algorithm briefly converges within the 5% error margin after exiting each red-shaded region, it soon produces spiked results in the general range of 5-25 seconds. However, this duration, in the green-shaded region, extends up to 45 seconds, and spiked results begin to appear.

4.4 Case 4

4.4.1 Test 7 - Vehicle at 3700 kg

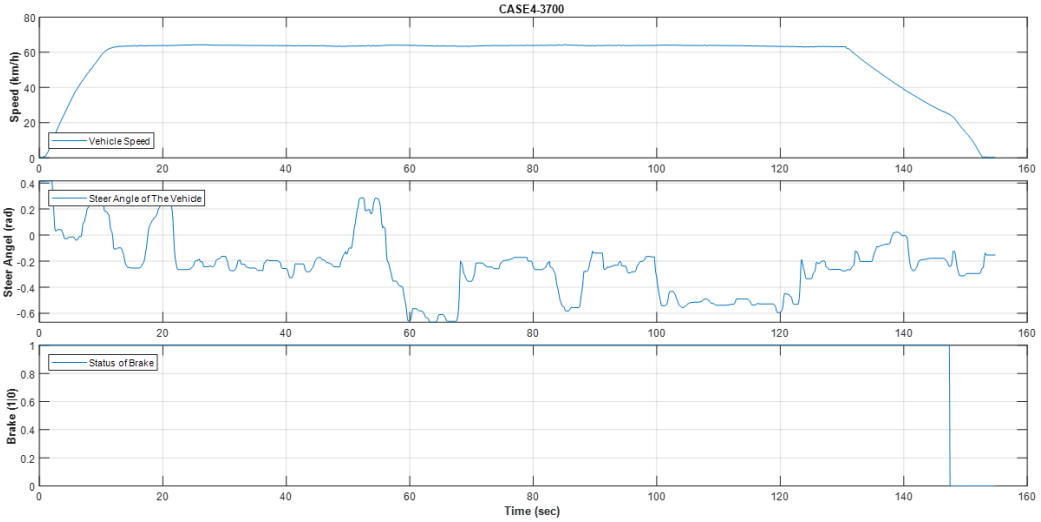

FIGURE 4.37: Speed, Steering Angle and Brake Profile of Test 7

In Case 4, an aggressive driving style was employed from the beginning, reaching the limited top speed in 12 seconds in Fig. 4.37. The vehicle then maintained a steady cruise for 118 seconds without deceleration. Subsequently, for approximately 17 seconds, the vehicle decelerated using regenerative braking, followed by brake application to complete the scenario defined in the same figure. During this test, the steering wheel was used in a range of +0.4 radians to the right and -0.65 radians to the left.

4.4.1.1 Gradient Descent

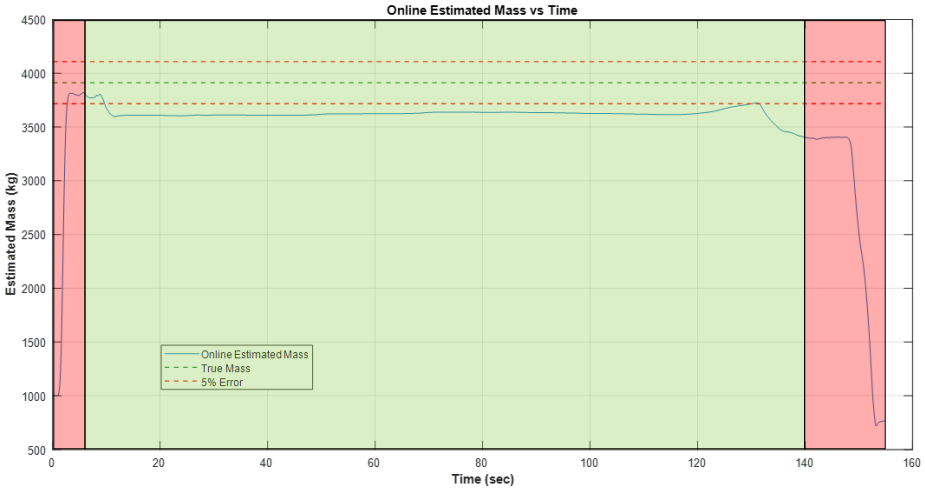

FIGURE 4.38: Mass Estimation Based on Gradient Descent Algorithm, Test 7

The estimation plot is characterized by a singular region that can be highlighted in green, as illustrated in Fig. 4.9, as there are no stop and go events or brake applications. The estimated mass is still outside the 5% error margin, despite the absence of abrupt turns or significant changes in acceleration. Between 120 and 140 seconds, the effect of regenerative braking on the algorithm is notably pronounced, as it substantially affects the estimation results.

4.4.1.2 Recursive Least Squares

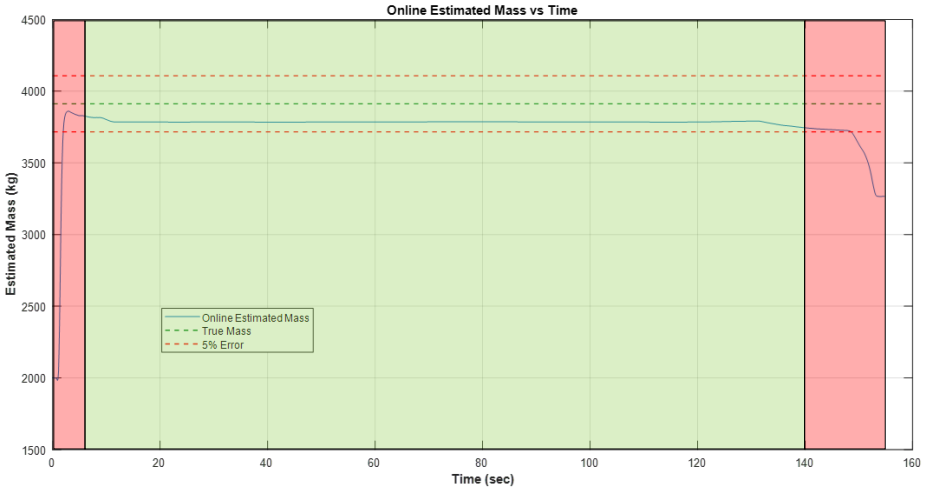

FIGURE 4.39: Mass Estimation Based on RLS Algorithm, Test 7

However, the estimation with RLS remains within the defined error margin, with an error of approximately 3.2%, as shown in Fig. 4.39. Compared to the Gradient Descent estimation in Case 4, the RLS algorithm demonstrates better performance.

4.4.1.3 Recursive Least Squares with a Single Forgetting Factor

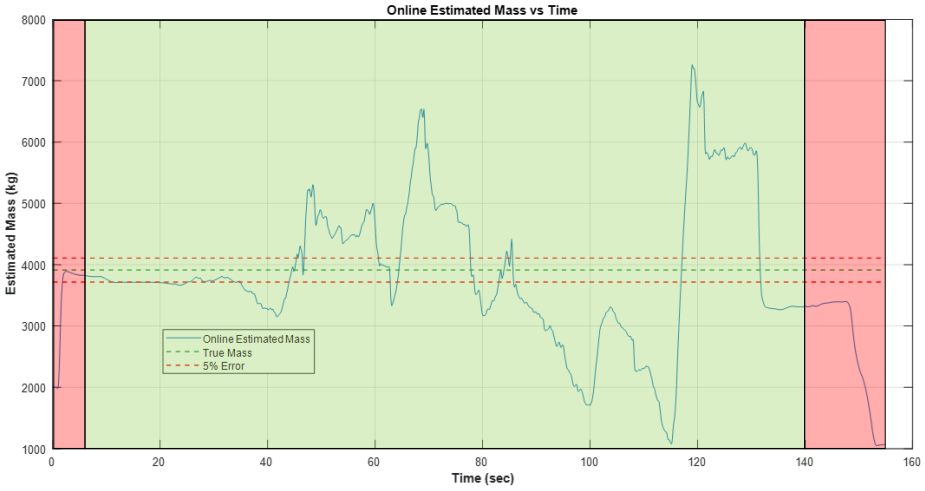

FIGURE 4.40: Mass Estimation Based on RLS with a Single Forgetting Factor Algorithm, Test 7

The RLS algorithm with a single forgetting factor initially operates within the 5% error margin but begins to produce unrealistic and inaccurate estimations after 33 seconds, as illustrated in Fig. 4.40. The design of Case 4 does not include any braking events or abrupt turns, which underscores the algorithm's inability to maintain accuracy under steady driving conditions.

4.4.1.4 Recursive Least Squares with a Multiple Forgetting Factor

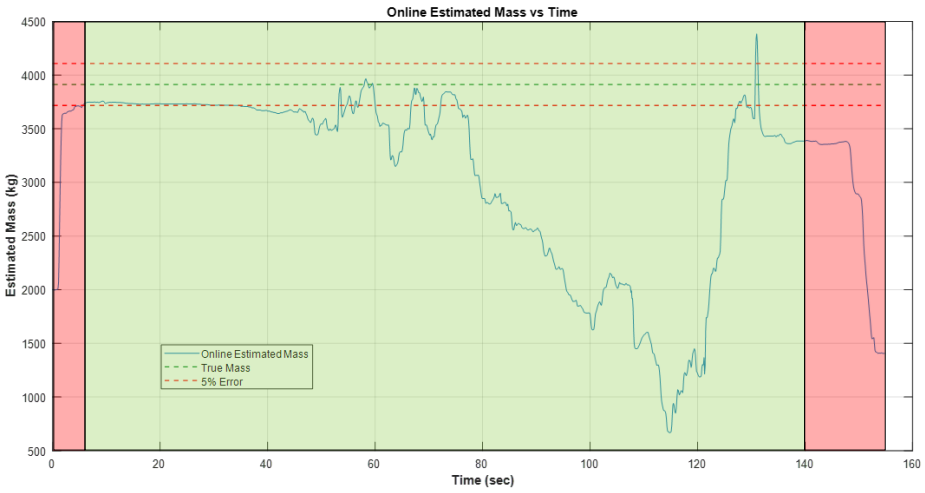

FIGURE 4.41: Mass Estimation Based on RLS with a Multiple Forgetting Factor Algorithm, Test 7

Similarly to the single one, multiple forgetting factor in Case 4, spikes begin to appear at 42 seconds, as shown in Fig. 4.40 and 4.41. However, a key difference between the RLS with a multiple forgetting factor and the single forgetting factor is that the error between the actual and estimated torque values is significantly lower in this case, indicating a better torque estimation. Nevertheless, this improvement in torque estimation does not guarantee an accurate mass estimation.

4.5 Case 5

4.5.1 Test 8 - Vehicle at 3700 kg

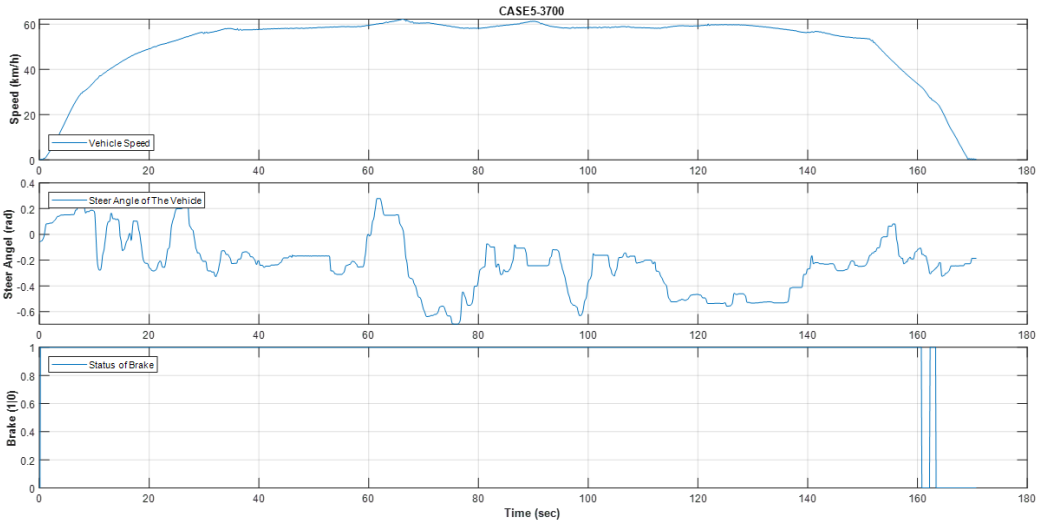

FIGURE 4.42: Speed, Steering Angle and Brake Profile of Test 8

The same track as in Case 4 was used; however, the driving style was different. As can be seen from the speed graph in Fig. 4.42, the driving style was designed to be more comfortable and oriented toward pleasure. Observed that the vehicle reaches a speed of 60 km/h between 35 and 37 seconds, whereas in Case 4, this was achieved in approximately 12 seconds. This indicates that the acceleration was more gradual, without fully depressing the accelerator pedal, ensuring a smoother experience for the passenger (copilot in certain cases) and the vehicle itself. Additionally, in Case 5, the vehicle completes the test at approximately 60 km/h, without reaching its maximum speed limit. The first-time brake was applied to slow the vehicle in the 16th second, whereas in Case 4, the vehicle had already come to a complete stop within the same time frame.

4.5.1.1 Gradient Descent

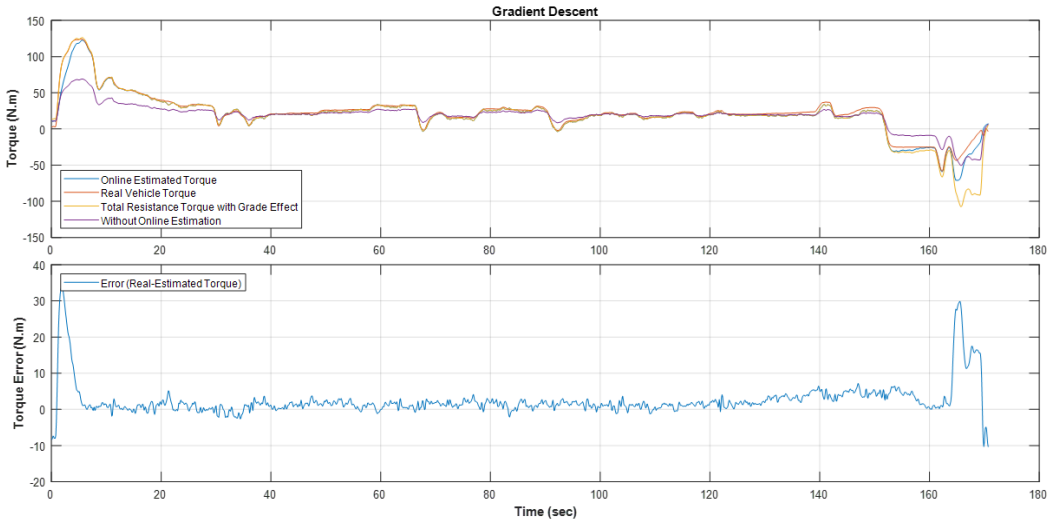

FIGURE 4.43: Torque Estimation Based on Gradient Descent Algorithm & Torque Error, Test 8

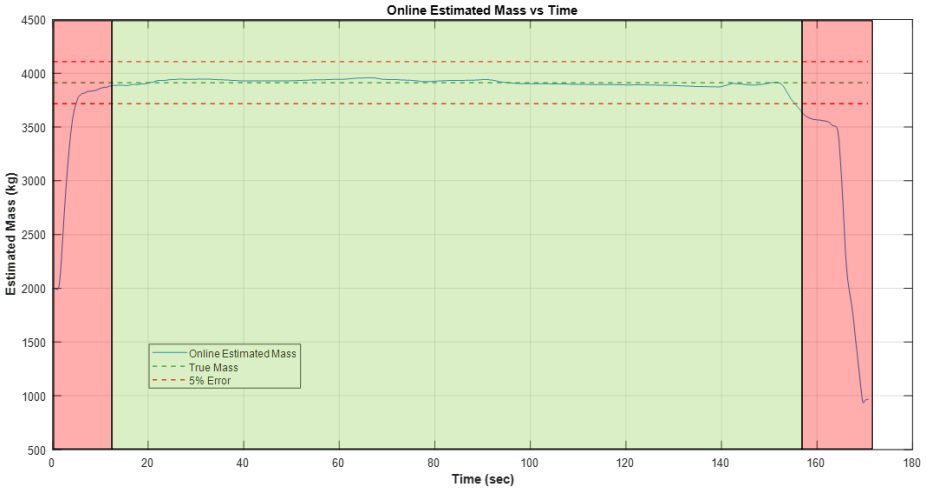

FIGURE 4.44: Mass Estimation Based on Gradient Descent Algorithm, Test 8

As shown in Fig. 4.44, the Gradient Descent algorithm in Case 5 performs exceptionally well, closely tracking the true mass with its estimations. In fact, within the green-shaded region, approximately 90% of the mass error remains within 1%. Furthermore, the algorithm quickly converges within the desired range, entering the error margin 5% even before reaching 60 km/h. However, toward the end of the green-shaded region, the influence of regenerative braking causes the estimations

to deviate, exceeding the defined error margin. This deviation is accompanied by a slight fluctuation in the torque error, as observed in Fig. 4.43, around the same time intervals.

4.5.1.2 Recursive Least Squares

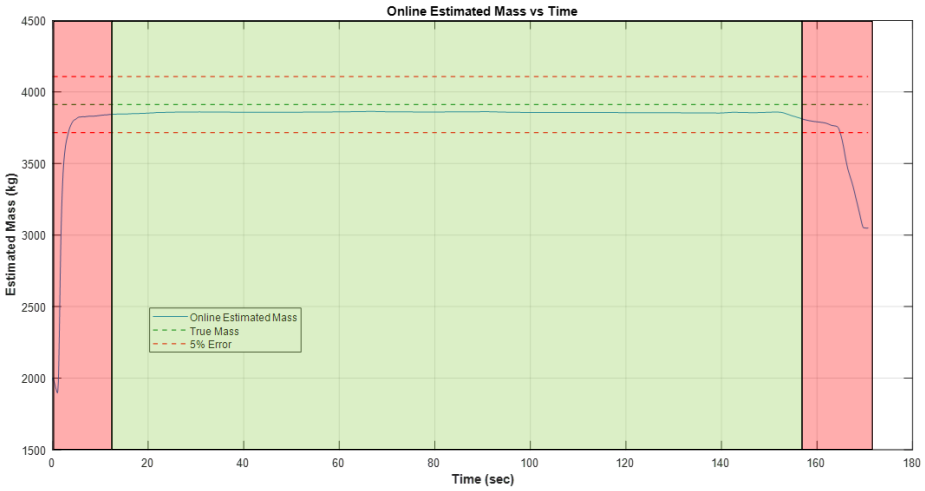

FIGURE 4.45: Mass Estimation Based on RLS Algorithm, Test 8

In the RLS algorithm, the mass estimation converges to the true mass much faster, reaching a steady-state condition even within the red-shaded region, as shown in Fig. 4.45. However, in the green-shaded region, the estimated mass remains at a noticeable distance from the true mass reference point compared to the same case's Gradient Descent performance.

4.5.1.3 Recursive Least Squares with a Single Forgetting Factor

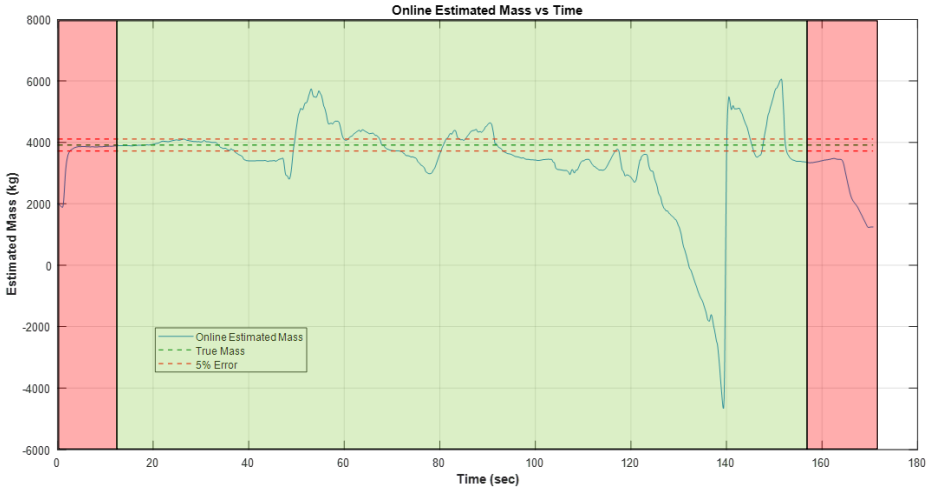

FIGURE 4.46: Mass Estimation Based on RLS with a Single Forgetting Factor Algorithm, Test 8

In a manner similar to the conventional RLS algorithm in Fig. 4.45, the mass estimation converges rapidly, preserving precise values until the 32th second, as illustrated in Fig. 4.46. Subsequently, it generates inconsistent estimations, resulting in implausible vehicle weight values. Significantly, at 140 seconds, the estimation falls below -4000 kg. In general, this indicates an overall insufficient estimation ability.

4.5.1.4 Recursive Least Squares with a Multiple Forgetting Factor

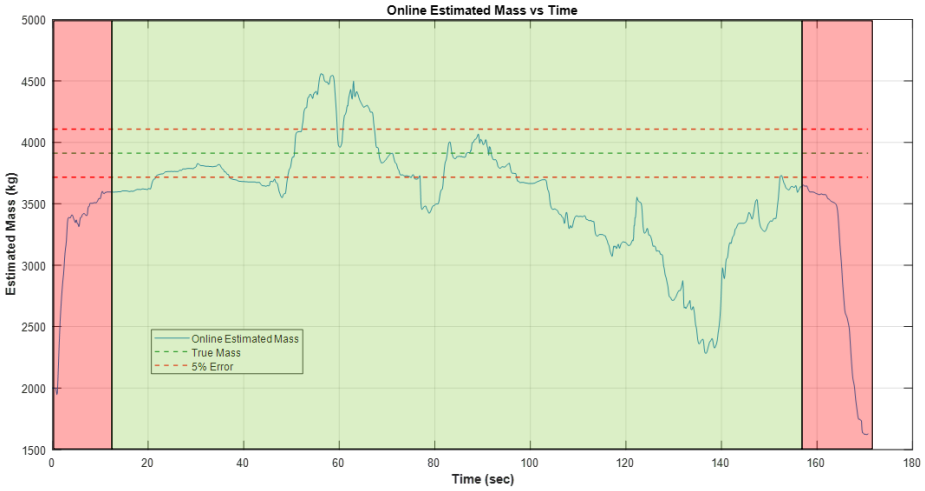

FIGURE 4.47: Mass Estimation Based on RLS with a Multiple Forgetting Factor Algorithm, Test 8

In Fig. 4.47, the estimated mass initially appears to converge toward the true mass in the 20-40 second interval at the beginning of the green-shaded region. Subsequently, it experiences a significant increase and fluctuations, with the estimated mass falling below 2500 kg. Despite some observed recovery attempts, the estimated mass does not converge with the true mass within the test duration.

Chapter 5

Discussion

Accurately predicting the consumption and range of electric vehicles is essential for extending their operational efficiency and addressing biases against their adoption. Improved range predictions can increase public interest in electric vehicles and play a critical role in meeting the EU Parliament's 2030 and 2050 sustainability goals.

Every vehicle is manufactured with a fixed weight when it leaves the factory, however, its weight can vary during use depending on the user's usage patterns, especially in commercial buses. In our study, assuming the full seating capacity of 13 passengers (driver included) is utilized and calculating the average weight of a

Case	KG	ID	Mass Estimation			Mass+Inclination Estimation
			Gradient Descent	**RLS**	**RLS w a Single Forgetting Factor**	**RLS w a Multiple Forgetting Factor**
1	**3700**	**Test 1**	2,1	6,1	8,4	5,7
	4200	**Test 2**	10,8	7,2	41,1	40,2
	4600	**Test 3**	3,3	19,4	26	28
	5000	**Test 4**	3,8	6,8	35,3	31,8
2	**3700**	**Test 5**	2,6	0,8	10,2	9,1
3	**3700**	**Test 6**	2,9	7	16,6	20,4
4	**3700**	**Test 7**	7,4	3,3	22,5	21,6
5	**3700**	**Test 8**	0,6	1,4	22,4	10,6

TABLE 5.1: Absolute Mean Errors for All Cases

person as 70 kg, an additional weight of 840 kg. This additional weight accounts for approximately 25% of the shuttle's curb weight of 3700 kg, as used in the tests. Furthermore, if standing passengers are considered, this percentage increases significantly. Unlike private cars, the weight of a bus fluctuates continuously along its route. Additionally, monitoring vehicle weight is critical for autonomous vehicles, as it directly impacts cornering, braking distances, and overall driving dynamics.

Grade effects are another significant factor influencing energy consumption predictions. As reported in [7], a 1% increase in road grade can result in up to a 15% rise in energy consumption. Previous studies, as discussed in Section 1.2, highlight the direct impact of grade variations on battery usage and range, emphasizing the importance of accurate grade estimation. Achieving accurate consumption and range predictions requires a robust understanding of vehicle and road dynamics to optimize control of vehicle parameters such as limiting the torque while inclination. This study evaluates the performance of four different algorithms, such as Gradient Descent, RLS, RLS with a Single Forgetting Factor, and RLS with multiple forgetting factors, in five scenarios/cases. These scenarios were specifically designed to examine the effects of traffic conditions, cornering, inclines, declines, and driving styles, as well as the influence of vehicle limitations on estimation accuracy.

AME values were calculated for all cases and tests based on the common intervals identified within each case across all algorithms. The results are presented in Tab. 5.1, where green highlights represent errors within the 5% margin, yellow indicates errors within the 5-10% range, and red denotes high AME values exceeding 10%. The Gradient Descent algorithm demonstrated the best overall performance, with AME values ranging from 0.6% to 3.8%, excluding Test 2 and Test 7. Its performance in Case 5, in particular, aligns closely with state-of-the-art studies. RLS ranked second, achieving an AME of 0.8% in Case 2, which was conducted on the original map in a scenario distinct from Case 1. Furthermore, RLS consistently outperformed Gradient Descent in torque estimation across nearly all cases.

In contrast, RLS with Single Forgetting Factor and RLS with Multiple Forgetting Factors produced less reliable results. The AME values for the single forgetting factor ranged between 8.4% and 41.1%, while the multiple forgetting factor produced values between 5.7% and 40.2%. Interestingly, the minimum and maximum AME values for both methods were observed in Test 1 and Test 2. Both algorithms frequently observed a tendency to drift toward unrealistic values in mass estimation, that can be seen in Sections 4.1.1 and 4.1.2.

Test 8 yielded the most accurate mass estimation results, while Test 2, produced the least accurate outcomes. The flat road and smooth driving style in Case 5 significantly contributed to its superior performance. The only difference between Cases 4 and 5 was the driving style, with the aggressive driving in Case 4 negatively impacting both torque and mass estimation. The software ensures that the vehicle does not exceed the specified limit when it reaches its maximum speed during aggressive driving. In this scenario, when the accelerator pedal is continuously pressed, the vehicle maintains its maximum speed by regulating motor torque and RPM accordingly. This situation applies to all scenarios where the maximum speed is reached, no matter whether the vehicle is ascending or descending. In the Case 1, it was observed that the uphill and downhill sections of the road caused torque and mass estimations to deviate significantly from the true values. The primary motivation for including Case 2 was to address the limitations observed in Case 1. In downhill segments, the estimations made in Case 2, particularly using the RLS algorithm, achieved results that can be described as state-of-the-art. In contrast, for the same downhill segment in Case 1, the lowest RLS AME value was 6.1%. A comparison between Case 1 and Case 2 reveals noticeable improvements across nearly all metrics.

For the grade estimation, open-source map data was used to obtain the reference values, which are deemed to be accurate, percentage plot of the grade gradient for the route in Case 1 is illustrated as in Fig. 2.13. Using two distinct sources of acceleration data—one derived from the brake ECU and the other calculated from the speed data obtained via motor RPM—we determined the percentage grade values, as shown in Fig. 4.2. We observed a correlation between the calculated

grade values and the open-source reference data. However, the numerical values did not fully align.

The study was conducted during the data collection procedure without using any extra sensors beyond the vehicle's standard configuration. Although the performance of the current sensors utilized in the study was satisfactory under specific situations, the integration of supplementary sensors like GNSS and IMU could significantly improve estimation accuracy, aligning the results with state-of-the-art references. Moreover, adding limitations on lateral dynamics and enhancing the estimate techniques could further reduce mistakes and elevate overall performance. Another potential area of study involves conducting a detailed analysis of the conditions under which the algorithm struggles to maintain stability and accuracy. This could include investigating the impact of vehicle dynamics and the limitations of the Master ECU on the algorithm's performance. By gaining a deeper understanding of the vehicle's behavior, we can achieve a more effective and reliable optimization of the system.

Chapter 6

Conclusion

Online gross-weight and road grade estimation for commercial passenger vehicles is an important step towards improving the fuel efficiency by the use of model-predictive control methods. This study investigated the performance of prediction-error-based estimation methods that do not require specialized computational and sensing hardware. The studied methods were compared by the estimation accuracy they achieved in the steady-state under various driving conditions typical for commercial vehicles. Our findings indicated that the recursive least square error methods with forgetting factors fail to provide reliable estimations in general. On the other hand, estimation error gradient based parameter updates or recursive least squares with no forgetting factor achieved an acceptable performance in most of the cases investigated. These promising methods assumed a measurement model for the road grade. Therefore, obtaining the road grade accurately appeared to be crucial in the success of these methods.

Additionally, the results indicated that the studied approaches are under performing when the vehicle decelerates rapidly or makes sharp and significant turns. This is primarily due to the fact that the estimation model utilized in this study was limited to the longitudinal dynamics of the vehicle. Incorporating the lateral dynamics to the estimation model could lift this performance barrier and enable appropriate performance in such driving conditions.

Apart from the possible improvements for the estimation methods, a crucial future work for this study would be the investigation of the impact of online estimation in electric commercial passenger vehicles such as the one used in this study. The sensitivity of fuel efficiency to the estimation performance under the conditions of city traffic can reveal the key performance qualifiers for estimation as well as model-based control of these vehicles.

Bibliography

[1] M. Zhao, F. Yang, D. Sun, W. Han, F. Xie, and T. Chen, "A joint dynamic estimation algorithm of vehicle mass and road slope considering braking and turning," in *2018 Chinese Control And Decision Conference (CCDC)*, pp. 5868–5873, 2018.

[2] M. N. Mahyuddin, J. Na, G. Herrmann, X. Ren, and P. Barber, "Adaptive observer-based parameter estimation with application to road gradient and vehicle mass estimation," *IEEE Transactions on Industrial Electronics*, vol. 61, no. 6, pp. 2851–2863, 2014.

[3] D. Incorporated, "Dana tm4 sumo family brochure," 2024. Accessed: 2024-12-18.

[4] B. Design, "Bmw i3 battery pack," 2024. Accessed: 2024-12-18.

[5] Plotaroute.com, "Plotaroute - route planner and gps route mapping tool," 2024. Accessed: 2024-12-15.

[6] Eurostat, "Primary energy consumption in the eu down by 3% in 2022," 2024. Accessed: 2024-12-18.

[7] S. Burgess and J. Choi, "A parametric study of the energy demands of car transportation: a case study of two competing commuter routes in the uk," *Transportation Research Part D: Transport and Environment*, vol. 8, no. 1, pp. 21–36, 2003.

[8] E. Hellström, M. Ivarsson, J. Åslund, and L. Nielsen, "Look-ahead control for heavy trucks to minimize trip time and fuel consumption," *Control Engineering Practice*, vol. 17, no. 2, pp. 245–254, 2009.

[9] I. Kim, H. Kim, J. Bang, and K. Huh, "Development of estimation algorithms for vehicle's mass and road grade," *International Journal of Automotive Technology*, vol. 14, pp. 889–895, Dec 2013.

[10] M. L. McIntyre, T. J. Ghotikar, A. Vahidi, X. Song, and D. M. Dawson, "A two-stage lyapunov-based estimator for estimation of vehicle mass and road grade," *IEEE Transactions on Vehicular Technology*, vol. 58, no. 7, pp. 3177–3185, 2009.

[11] A. S. A. Vahidi and H. Peng, "Recursive least squares with forgetting for online estimation of vehicle mass and road grade: theory and experiments," *Vehicle System Dynamics*, vol. 43, no. 1, pp. 31–55, 2005.

[12] N. Lin, C. Zong, and S. Shi, "The method of mass estimation considering system error in vehicle longitudinal dynamics," *Energies*, vol. 12, no. 1, 2019.

[13] P. Lingman and B. Schmidtbauer, "Road slope and vehicle mass estimation using kalman filtering," *Vehicle System Dynamics*, vol. 37, no. sup1, pp. 12–23, 2002.

[14] V. Winstead and I. Kolmanovsky, "Estimation of road grade and vehicle mass via model predictive control," in *Proceedings of 2005 IEEE Conference on Control Applications, 2005. CCA 2005.*, pp. 1588–1593, 2005.

[15] X. Zhang, L. Xu, J. Li, and M. Ouyang, "Real-time estimation of vehicle mass and road grade based on multi-sensor data fusion," in *2013 IEEE Vehicle Power and Propulsion Conference (VPPC)*, pp. 1–7, 2013.

[16] S. De Bruyne, H. Van der Auweraer, P. Diglio, and J. Anthonis, "Online estimation of vehicle inertial parameters for improving chassis control systems," *IFAC Proceedings Volumes*, vol. 44, no. 1, pp. 1814–1819, 2011. 18th IFAC World Congress.

[17] S. Torabi, M. Wahde, and P. Hartono, "Road grade and vehicle mass estimation for heavy-duty vehicles using feedforward neural networks," in *2019 4th International Conference on Intelligent Transportation Engineering (ICITE)*, pp. 316–321, 2019.

[18] A. H. Korayem, A. Khajepour, and B. Fidan, "Trailer mass estimation using system model-based and machine learning approaches," *IEEE Transactions on Vehicular Technology*, vol. 69, no. 11, pp. 12536–12546, 2020.

[19] K. Automotive, "Karsan otomotiv resmi web sitesi," 2024. Accessed: 2024-12-15.

[20] A. Ritter, F. Widmer, B. Vetterli, and C. H. Onder, "Optimization-based online estimation of vehicle mass and road grade: Theoretical analysis and experimental validation," *Mechatronics*, vol. 80, p. 102663, 2021.

[21] M. Ehsani, Y. Gao, S. E. Gay, and A. Emadi, *Modern Electric, Hybrid Electric, and Fuel Cell Vehicles: Fundamentals, Theory, and Design*. Power Electronics and Applications Series, Boca Raton, FL: CRC Press, 2004. Library of Congress Control Number: 2004054249.

[22] C. Electronics, "Can bus explained - a simple introduction (2024 tutorial)," 2024. Accessed: 2024-12-15.

[23] Plotaroute.com, "Route planner: Route 2670389." `https://www.plotaroute.com/route/2670389?units=km`, 2024. Accessed: 2024-12-15.

[24] Plotaroute.com, "Route planner: Route 2785593." `https://www.plotaroute.com/route/2785593?units=km`, 2024. Accessed: 2024-12-15.

[25] J.-J. E. Slotine, "Applied nonlinear control," *PRENTICE-HALL google schola*, vol. 2, pp. 1123–1131, 1991.